August 2019

[Accepted Article Manuscript Version (Postprint)] Metabolic Alterations in the Enoyl-CoA Hydratase 2 Mutant Disrupt Peroxisomal Pathways in Seedlings

Bethany Zolman
University of Missouri-St. Louis, zolmanb@umsl.edu

Ying Li
yl74b@mail.umsl.edu

Yu Liu

Metabolic Alterations in the Enoyl-CoA Hydratase 2 Mutant Disrupt Peroxisomal Pathways in Seedlings[1][OPEN]

Ying Li, Yu Liu, and Bethany K. Zolman[2,3]

University of Missouri–St. Louis, St. Louis, Missouri 63121

ORCID IDs: 0000-0001-9714-8156 (Y.L.); 0000-0001-6070-7989 (B.K.Z.).

Mobilization of seed storage compounds, such as starch and oil, is required to provide energy and metabolic building blocks during seedling development. Over 50% of fatty acids in Arabidopsis (*Arabidopsis thaliana*) seed oil have a cis-double bond on an even-numbered carbon. Degradation of these substrates requires peroxisomal fatty acid β-oxidation plus additional enzyme activities. Such auxiliary enzymes, including the enoyl-CoA hydratase ECH2, convert (R)-3-hydroxyacyl-CoA intermediates to the core β-oxidation substrate (S)-3-hydroxyacyl-CoA. ECH2 was suggested to function in the peroxisomal conversion of indole-3-butyric acid (IBA) to indole-3-acetic acid, because *ech2* seedlings have altered IBA responses. The underlying mechanism connecting ECH2 activity and IBA metabolism is unclear. Here, we show that *ech2* seedlings have reduced root length, smaller cotyledons, and arrested pavement cell expansion. At the cellular level, reduced oil body mobilization and enlarged peroxisomes suggest compromised β-oxidation. *ech2* seedlings accumulate 3-hydroxyoctenoate (C8:1-OH) and 3-hydroxyoctanoate (C8:0-OH), putative hydrolysis products of catabolic intermediates for α-linolenic acid and linoleic acid, respectively. Wild-type seedlings treated with 3-hydroxyoctanoate have *ech2*-like growth defects and altered IBA responses. *ech2* phenotypes are not rescued by Suc or auxin application. However, *ech2* phenotypes are suppressed in combination with the core β-oxidation mutants *mfp2* or *ped1*, and *ech2 mfp2* seedlings accumulate less C8:1-OH and C8:0-OH than *ech2* seedlings. These results indicate that *ech2* phenotypes require efficient core β-oxidation. Our findings suggest that low ECH2 activity causes metabolic alterations through a toxic effect of the accumulating intermediates. These effects manifest in altered lipid metabolism and IBA responses leading to disrupted seedling development.

The earliest stages of plant development, including germination and seedling establishment, are critical transition points for dormant seeds to mature into flowering plants. Proper development requires the close coordination and tight regulation of multiple physiological pathways. For instance, mobilization of storage compounds, such as starch and oil, is required to provide both energy and metabolic building blocks. Meanwhile, hormonal signals direct the growth and define the morphology of developing plants in conjunction with environmental signals.

Triacylglycerol (TAG) is the major storage compound in oilseed plants. In Arabidopsis (*Arabidopsis thaliana*), 35–40% of seed dry weight comprise oil (Li-Beisson et al., 2010), which is packed in oil bodies. Oil bodies are synthesized from the endoplasmic reticulum in embryonic cells and accumulate in dry seeds (Kim et al., 2013). Upon germination, storage lipids are quickly consumed to provide energy and metabolic substrates for seedling development before photosynthesis initiates. The consumption of oil bodies begins with the release of free fatty acids (FFAs) via TAG hydrolysis by the lipase SDP1 (SUC DEPENDENT1; Eastmond, 2006). FFAs are used either in membrane biogenesis or metabolized through β-oxidation in peroxisomes, which are organelles housing oxidative reactions.

Many proteins are required for fatty acid catabolism (Fig. 1). The import of fatty acyl-Coenzyme A (acyl-CoA) esters by the ATP-dependent transporter PXA1/CTS/PED3 (PEROXISOMAL ABC TRANSPORTER/COMATOSE/PEROXISOME DEFECTIVE) is coupled with CoA-hydrolysis (Zolman et al., 2001; Footitt et al., 2002; Hayashi et al., 2002; Nyathi et al., 2010; De Marcos Lousa et al., 2013). Inside the organelle, fatty acids are re-esterified with CoA by the long-chain acyl-CoA synthetases (LACS) LACS6 and LACS7 (Fulda et al., 2004). The activated acyl-CoA is oxidized at its β-carbon by acyl-CoA oxidase (ACX1-ACX6), followed by sequential hydration, dehydrogenation, and thiolytic cleavage steps catalyzed by a multifunctional protein (MFP2 or AIM1) and 3-ketoacyl-CoA thiolase (KAT1, KAT2/PED1, and KAT5), respectively (for review, see Kao et al., 2018). These enzyme activities comprise the core β-oxidation cycle. Overall, the acyl-CoA chain is shortened by two carbons during each round of β-oxidation. The two carbons are released as

[1]This work was supported by the HHS National Institutes of Health (NIH) (1R15GM116090-01) and the University of Missouri Research Board.

[2]Author for contact: zolmanb@umsl.edu.

[3]Senior author

The author responsible for distribution of materials integral to the findings presented in this article in accordance with the policy described in the Instructions for Authors (www.plantphysiol.org) is: Bethany K. Zolman (zolmanb@umsl.edu).

Y.L. and B.K.Z. designed the project; Y. Li and Y. Liu performed the experiments and analyzed the data; all authors wrote the article.

[OPEN]Articles can be viewed without a subscription.

www.plantphysiol.org/cgi/doi/10.1104/pp.19.00300

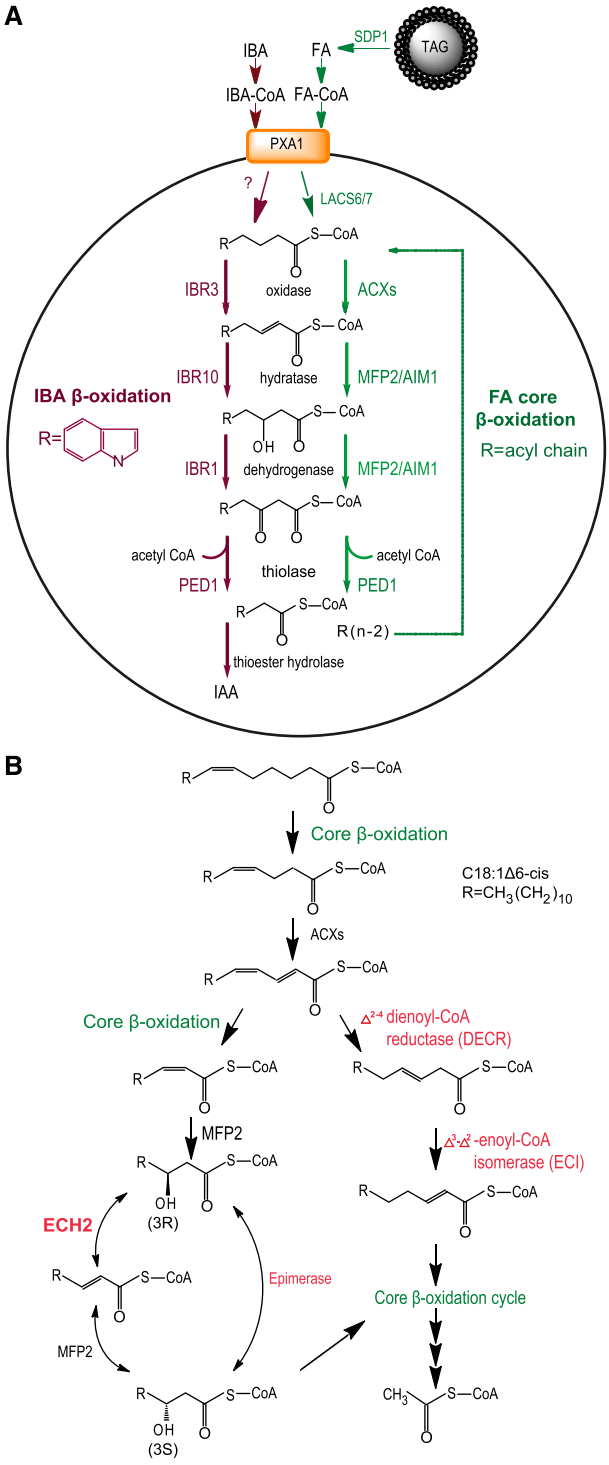

Figure 1. Peroxisomal β-oxidation of fatty acids and IBA. A, Fatty acids (green) and IBA (purple) are processed and transported to peroxisomes for catabolism through β-oxidation. Required enzyme activities are indicated in the center of the mechanism; known or predicted enzymes acting in each pathway are indicated outside the arrows. The enzyme converting IBA to IBA-CoA is unknown, and it is not clear if IBA is transported into peroxisome in the form of IBA or IBA-CoA. B, The complete degradation of C18:1Δ6-cis is shown as an example of pathways involved in catabolism of fatty acids with a cis-double bond on an even-numbered carbon. Auxiliary enzymes are in red. The first double bond of unsaturated fatty acids is always more than two carbons away from the CoA attachment site. Thus, at least one round of core β-oxidation is required to function upstream of auxiliary pathways in the metabolism of unsaturated fatty acids.

acetyl-CoA, which can be condensed to 4-carbon compounds via the peroxisomal glyoxylate cycle. These compounds can be used as carbon skeletons, as well as the precursor of hexose and Suc (with the integration of cytosolic and mitochondrial metabolism) to support cell wall biosynthesis and fuel seedling growth (for review, see Graham, 2008; Böttcher and Pollmann, 2009). Mutants defective in fatty acid β-oxidation enzymes result in developmental abnormalities or growth retardation. Mutants with strong defects have arrested seedling establishment, whereas partial loss-of-function lines have short roots and hypocotyls; these phenotypes can be rescued by application of Suc as an exogenous carbon source, which precludes the need for β-oxidation metabolites (Hayashi et al., 1998; Hu et al., 2012).

Saturated fatty acids are catabolized through the core β-oxidation spiral after CoA attachment. However, a large proportion of fatty acids in seed storage oils are unsaturated, which require additional auxiliary peroxisomal activities for degradation. For example, Figure 1B shows the complete degradation of petroselinic acid, a fatty acid with 18 carbons and one double bond in the cis-configuration at an even-numbered (Δ6) carbon (C18:1Δ6-cis). Following core β-oxidation, degradation of unsaturated molecules occurs via one of two auxiliary pathways: the reductase/isomerase pathway or the hydratase/epimerase pathway (for review, see Graham, 2008). For the reductase/isomerase pathway, 2, 4-dienoyl-CoA reductase (DECR) activity has been detected in Arabidopsis and a putative gene *DECR/SDRB* was identified (Reumann et al., 2007). Three Arabidopsis genes were identified that encode Δ3, Δ2-enoyl-CoA isomerases (AtECI1-3), whose activities were characterized when expressed heterologously in yeast (Goepfert et al., 2008). The alternative hydratase/epimerase pathway requires a 3-hydroxyacyl-CoA epimerase and two stereo-specific enoyl-CoA hydratases. The 3-hydroxyacyl-CoA epimerase activity was characterized initially in cucumber (Preisig-Müller et al., 1994) and may be completed by one of the multifunctional enzymes in other plants (Graham, 2008). MFP2 and ECH2 confer the stereospecific enoyl-CoA hydratase 1 and 2 activity, respectively. Analysis of the carbon flux in the β-oxidation pathway of *AtECH2* RNA interference (RNAi) lines suggested ECH2 converts (R)-3-hydroxyacyl-CoA intermediates to the (S)-3-hydroxyacyl-CoA core β-oxidation intermediates (Goepfert et al., 2006).

Mutant analysis revealed that ECH2 activity in mobilizing storage lipids is important for cell expansion and proliferation (Strader et al., 2011; Katano et al., 2016). Interestingly, *ech2-1* phenotypes also suggested

the involvement of ECH2 in the metabolism of Indole-3-butyric acid (IBA), a precursor and potential storage form of indole-3-acetic acid (IAA; Strader et al., 2011). IAA affects plant growth and development by directing cell division and elongation (Velasquez et al., 2016; Majda and Robert, 2018). The conversion of IBA to IAA is achieved through removal of two carbons from the butanoate side chain, a β-oxidation-like pathway also occurring in peroxisomes (Zolman et al., 2000; Strader et al., 2011). Enzymes acting in IBA to IAA conversion were identified through forward genetic screening for mutants that are resistant to the inhibition effect of IBA on root and/or hypocotyl elongation, known as IBA-response (*ibr*) mutants (Zolman et al., 2000; Strader et al., 2011). Based on sequence homology to characterized enzymatic domains, IBR3, IBR10, and IBR1 were predicted to act at successive steps of the IBA β-oxidation pathway (Fig. 1A; Zolman et al., 2007, 2008). ECH2 has been hypothesized to act at the enoyl-CoA hydratase step and/or the IAA-CoA hydrolase step, because ECH2 also contains a hot dog domain associated with potential thioesterase activity (Strader et al., 2011). Additionally, the PED1 thiolase was predicted to have overlapping functions on IBA to IAA conversion based on the IBA-resistant phenotype of a *ped1* mutant (Lingard and Bartel, 2009). Genetic evidence indicates that IBA-derived IAA is important in germination, root branching, and cell expansion for both roots and leaves (Zolman et al., 2008; Strader et al., 2011; Spiess et al., 2014).

Here, we have investigated the role of ECH2 in fatty acid metabolism and IBA to IAA conversion further to better understand how peroxisomal processes are orchestrated to regulate the early developmental stages of plants. Metabolic profiling of *ech2* reveals an over-accumulation of (R)-3-hydroxy-5-octenoic acid, a putative hydrolysis product of the presumed ECH2 substrate for α-linolenic acid (ALA) catabolism. Epistasis analysis of mutants disrupting ECH2 and other lipid catabolism enzymes has revealed a link between β-oxidation efficiency, over-accumulation of pathway intermediates, and altered growth phenotypes and IBA responses.

RESULTS

ech2 Has Altered Seedling Development, But Normal Adult Growth

Arabidopsis development requires the concerted effort of fatty acid metabolism and hormone signaling. We examined the effects of disrupting IBA to IAA conversion and fatty acid catabolism activity on seedlings. Mutants defective in each pathway were examined for cotyledon growth and primary root elongation. The tested IBA-response (*ibr*) mutants included *ibr1*, *ibr3*, *ibr10*, and *ech2*. For fatty acid catabolism, *acx3*, *mfp2*, *aim1*, and *ped1* were used. Each line was grown on Suc-containing media for 7 d. Only *ech2* showed obviously reduced cotyledon size and primary root length (Fig. 2; Supplemental Fig. S1). Moreover, *ech2* cotyledons had reduced pigmentation compared with wild-type seedlings (Fig. 2A; Supplemental Fig. S1). However, true leaves and the overall size of *ech2* rosettes were comparable with that of wild type (Fig. 2, C and D). These results suggest that decreased ECH2 activity disrupts normal cotyledon development, but this defect has a reduced effect during adult development. The altered seedling development of *ech2* was rescued in transgenic plants overexpressing *ECH2* (Supplemental Fig. S2, A and B).

Similar seed weight and germination rate between wild type and *ech2* (Supplemental Fig. S3) suggest embryonic defects are unlikely the cause of retarded *ech2* development. Thus, we hypothesize the seedling growth phenotype can be attributed to compromised postgermination development. The normal growth of true leaves in *ech2* suggests that the heterotrophic nature of early seedling development may be a key to cause the growth defect.

ech2 Cotyledons Have Reduced Pavement Cell Area and Complexity

To characterize the defects of *ech2* in cotyledon development, pavement cells were imaged at d 5 and 12. Notably, *ech2* pavement cells not only had reductions in cell area, but also in the levels of interlocking with adjacent cells. Wild-type pavement cells are shaped like a jigsaw puzzle of interlocked pieces with lobes (convex) and indentations (concave). *Ech2* pavement cells were shaped more like irregular rectangles, with few lobes and indentations (Fig. 2E). Circularity was used as an index for complexity of pavement cells based on the independence of cell area (Zhang et al., 2011). A higher circularity indicates less complexity. In both wild-type and *ech2* cotyledon pavement cells, increased cell area, with more lobes and indentations, was noted at d 12 compared to d 5 (Fig. 2F). However, the circularity of *ech2* cotyledon pavement cells was consistently higher than that of wild type, indicating *ech2* has reduced pavement cell complexity throughout cotyledon development (Fig. 2F). Notably, pavement cells in the *ech2* true leaves were comparable with that of wild type in area and lobe number, consistent with normal growth of *ech2* beginning with the first true leaves (Fig. 2F). Transgenic complementation lines also showed restoration of cell patterning (Supplemental Fig. S2C), consistent with the restoration of cotyledon size noted above.

Lobe and indentation formation involves two antagonistic Rho GTPase signaling pathways (Feiguelman et al., 2018). ROP2 and ROP4 activate the effector RIC4 to promote cortical diffusion of F-actin and outgrowth of lobes. ROP6 suppresses ROP2, activating the effector RIC1 to promote microtubule organization and indentation formation (Fu et al., 2005). *Ech2* pavement cell morphology resembled that of a mutant disrupted in both *ROP2* and *ROP4* (Xu et al., 2010). To test if the Rho GTPase signaling pathway is compromised in *ech2*,

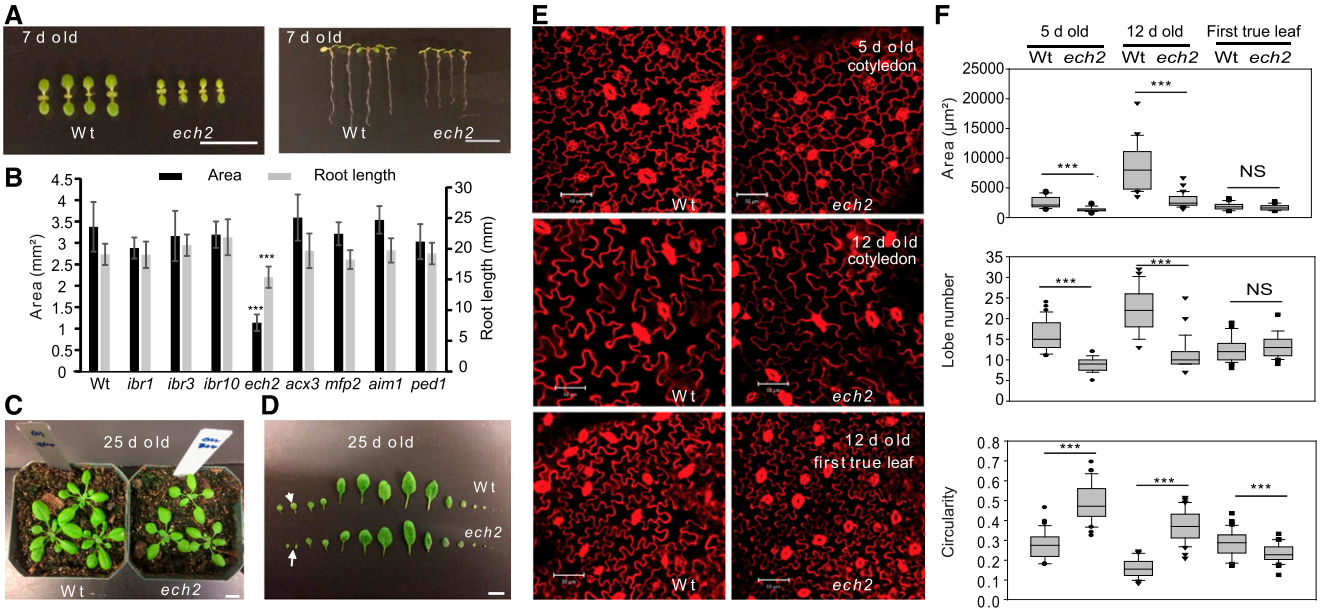

Figure 2. *ech2* has altered seedling development, but normal adult growth. A, Left, cotyledons of 7-d-old wild-type (Wt) and *ech2* seedlings. Right, images of whole seedlings. Bar = 1 cm. B, Mean cotyledon area and root length (± SD; $n \geq 10$) of 7-d-old wild type, i*br1-2*, *ibr3-1*, *ibr10-1*, *ech2-1*, *acx3-6*, *mfp2-2*, and *ped1-96* seedlings. Bar = 1 cm. ***$P < 0.005$ in Students' *t* test between wild type and mutants. C, Morphology of 25-d-old wild-type and *ech2* plants. Bar = 1 cm. D, Leaf spread of 25-d-old wild-type (top) and *ech2* (bottom) plants in order of emergence. White arrows designate the cotyledons. Bar = 1 cm. E, Representative confocal microscopy images of propidium iodide-stained wild type and *ech2* cotyledon pavement cells at d 5 (top) and d 12 (middle), and the first true leaf pavement cells at d 12 (bottom). Bar = 50 μm. F, The area, lobe number, and circularity of pavement cells. Circularity = 4π(area)/(perimeter)^2; the value of circularity is between 0 and 1. A value of 1 indicates a perfect circle; 0 indicates a shape with infinite complexity. Data are shown ± SD; $n > 30$. ***$P < 0.005$ in Students' *t* test between wild type and *ech2*. NS, not significant.

expression levels of *ROP2*, *ROP4*, and *ROP6* along with the *RIC4* and *RIC1* effectors were examined in cotyledons and true leaves. Consistently, *ROP2* and *ROP4* were down-regulated in *ech2* seedlings at d 3 when cotyledons emerged (~2-fold lower than wild type), but not at d 25, when true leaves were well developed (Supplemental Fig. S4, A and B). *RIC4* expression levels paralleled those of *ROP2* and *ROP4* at d 3. These results suggest that the reduced complexity of *ech2* cotyledon pavement cells might be related to compromised Rho GTPase signaling.

Despite *ech2-1* having defects in IBA responses, auxin application did not rescue the complexity or the area of the *ech2* cotyledon pavement cells (Supplemental Fig. S5). Although a negative result in this experiment is not definitive of a direct contribution, our results suggested contributors other than reduced IBA-derived IAA levels in *ech2* disrupt cotyledon development and led us to explore other metabolic pathways in more detail.

ech2 Shows Reduced Fatty Acid Catabolism

β-Oxidation mutants typically have improved growth in the presence of Suc (Germain et al., 2001; Pinfield-Wells et al., 2005; Rylott et al., 2006; Thazar-Poulot et al., 2015). Exogenous Suc supplants the need for lipid metabolism and promotes growth and development. We examined *ech2* Suc dependence as a first step in characterizing its β-oxidation activity. We compared seedlings grown on medium with or without Suc under light and dark conditions. In the light, *ech2* had improved cotyledon and primary root development when Suc was added (Supplemental Fig. S6), suggesting the beneficial effect of Suc as energy source and carbon supply on *ech2* seedling establishment. Although not completely restored, growth was more similar to wild type. On the contrary, under darkness, *ech2* showed similar hypocotyl elongation regardless of the presence of Suc (Supplemental Fig. S7). These results indicate that Suc affects seedling development of *ech2* only when light is present, unlike the well-characterized β-oxidation mutants *mfp2* and *ped1* (Supplemental Fig. S7; Rylott et al., 2006; Lingard and Bartel, 2009).

We next visualized potential disruptions of fatty acid metabolism in *ech2* by examining oil bodies and peroxisomes with confocal microscopy. Many fatty acid β-oxidation mutants with impaired lipid mobilization retain oil bodies and have enlarged peroxisomes, including *mfp2* and *ped1* (Rinaldi et al., 2016). We visualized and counted oil bodies in wild-type and *ech2* cotyledon pavement cells. Oil bodies in wild-type cotyledon pavement cells were abundant on d 3, but significantly fewer on d 4 and d 5 (Fig. 3A). On d 3, the total oil body area, as indicated by oil body

fluorescence, was more in *ech2* than that in wild type. The number of oil bodies in *ech2* was comparable with wild-type samples (Fig. 3B), suggesting that oil bodies in *ech2* were either larger or aggregated. At d 4 and d 5, however, *ech2* not only had increased oil body area, but also an increased number relative to wild type, although the trend of mobilization over time remained consistent in *ech2* samples. Peroxisomes also were imaged in wild-type and *ech2* seedlings expressing a peroxisomally targeted GFP (Woodward and Bartel, 2005). The number of peroxisomes in cotyledon pavement cells decreased on d 5 compared with d 4 in both wild type and *ech2*. However, more peroxisomes were present in *ech2*, and the overall organelle size was larger than in wild type (Fig. 3, C and D). These results suggest retarded lipid mobilization when ECH2 function is disrupted.

To characterize the effect of losing ECH2 enoyl-CoA hydratase activity on acyl-CoA oxidase products in core β-oxidation reactions, electrospray ionization tandem mass spectrometry (ESI-MS/MS) was used. CoA conjugated intermediates were quantified from β-oxidation reactions using extracts from 3-d-old seedlings with an acyl-CoA (C18:1, n-9) substrate. Supplemental Figure S8 shows the relative abundance of C18:1 (n-9) substrate and the resulting 2-trans-enoyl-CoA, 3-hydroxyacyl-CoA, and 3-ketoacyl-CoA intermediates. Accumulation of 2-transenoyl-CoA, the potential ECH2 substrate, was significantly higher in *ech2* than in wild type (~ 1.4 fold). In contrast, accumulation of 3-hydroxyacyl-CoA, the presumed ECH2 product, was significantly lower in *ech2* than in wild type (0.55-fold). Increased upstream substrates coupled with reduced products indicate that β-oxidation was reduced in *ech2*. Although these results suggest that the mutation compromises ECH2 enoyl-CoA hydratase activity on acyl-CoA oxidase products, a large amount of substrate is processed properly. Further, the changes are not to the degree of defects seen in *mfp2* mutant lines (Rylott et al., 2006) and suggest a minor role for ECH2 in the core β-oxidation pathway.

Efficient Core β-Oxidation and TAG Hydrolysis Are Required for *ech2* Phenotypes

To test if *ECH2* loss affects mutants defective in other peroxisomal pathways, higher-order mutants were analyzed. Previous work demonstrated that *ibr1 ibr3*

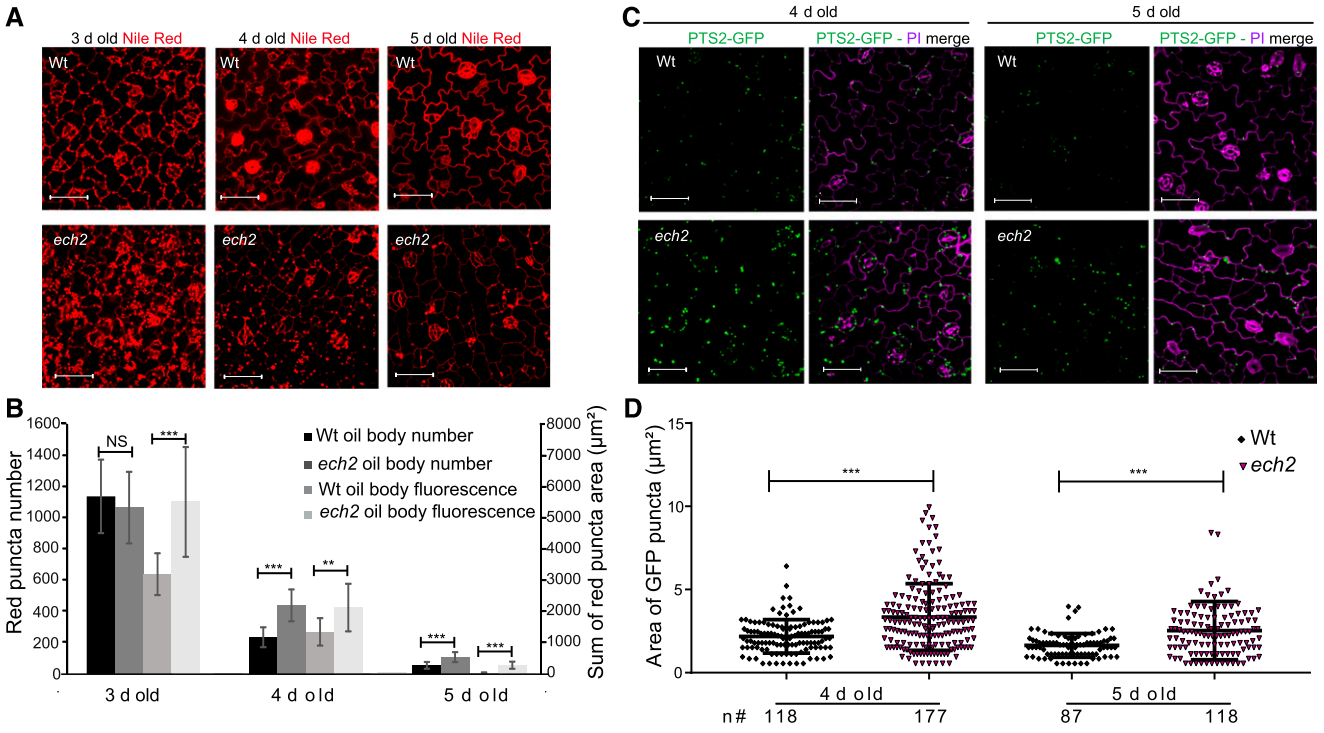

Figure 3. *ech2* has reduced oil body mobilization and enlarged peroxisomes. A, Confocal microcopy of cotyledon pavement cells in 3, 4, and 5-d-old wild-type (Wt) and *ech2* seedlings. Nile red was used to stain oil bodies (red). B, Nile-red puncta number and sum of nile-red puncta areas per 202.5 × 202.5 μm image (± SD; $n = 10$). C, Confocal microcopy of peroxisomes in cotyledon pavement cells of 4- and 5-d-old wild-type and *ech2* seedlings expressing peroxisomally targeted GFP (PTS2-GFP). Propidium iodide was used to stain pavement cell membranes (magenta). D, PTS2-GFP puncta areas from 202.5 × 202.5 μm images shown in (C) were plotted (± SD; $n > 100$). ***$P < 0.005$ in Students' t test. The number below the x axis indicates how many puncta were measured for wild type and *ech2* on each day. Results shown are representative of four independent experiments. For all panels, scale bar = 50 μm.

ibr10 ech2 displayed similar small cotyledons to *ech2* (Strader et al., 2011). The same response was observed in other *ibr* mutant combinations containing *ech2* (Supplemental Fig. S9A). However, *ech2 mfp2* did not have a size reduction and showed comparable cotyledon area to wild-type and the *mfp2* parent lines (Fig. 4). Notably, the small cotyledons of *ibr1 ibr10 ech2* also were rescued by incorporation of *mfp2* (Supplemental Fig. S9B). These results demonstrate that loss of MFP2 can suppress the defects associated with ECH2 dysfunction regardless of IBA to IAA conversion levels. Pavement cells in *ech2 mfp2* cotyledons were of similar area and complexity to wild type and *mfp2* (Fig. 4, B–D), suggesting that *mfp2* suppresses the *ech2* defects in cotyledon development by promoting cotyledon cell expansion.

Previous studies suggested *ech2* had reduced levels of IBA-derived IAA, as it produced fewer lateral roots and developed shorter root hairs than wild type (Strader et al., 2011). This phenotype also was suppressed by combination with *mfp2*, as *ech2 mfp2* produced more lateral roots and developed longer root hairs than *ech2* (Fig. 5). Similarly, IBA responses were tested based on the resistance of dark-grown seedlings to the inhibitory effects of IBA on hypocotyl elongation. Figure 5, E and F, shows that *ech2 mfp2* showed IBA sensitivity in hypocotyl growth compared with *ech2*, further supporting a suppressive effect of *mfp2* on *ech2* phenotypes. These results suggest that *mfp2* suppressed the IBA to IAA conversion defects associated with losing ECH2 activity.

Phenotypic assays also were done on combination lines incorporating other core β-oxidation mutants. Incorporation of *ped1* with *ech2* showed identical responses as *mfp2* combination (Fig. 4A; Supplemental Fig. S9B), supporting the above model that the direct disruption of fatty acid β-oxidation rescues *ech2* mutant phenotypes. Similarly, analysis of *ech2 sdp1*, which also disrupts TAG lipase, showed that *sdp1* suppresses *ech2* phenotypes (Supplemental Fig. S10, A and B). However, *ech2 acx3* and *ech2 aim1* combination mutants showed morphology similar to *ech2* (Supplemental Fig. S10C). *mfp2* and *ped1* have stronger reductions in fatty acid metabolism than *acx3* and *aim1* (Supplemental Fig. S7; Rylott et al., 2006; Lingard and Bartel, 2009). As demonstrated previously, phenotypes in *acx* mutant lines and *aim1* can be masked by redundancy, expression domains, and substrate specificity (Rylott et al., 2003; Adham et al., 2005; Wiszniewski et al., 2009; Khan et al., 2012). For these reasons, we hypothesize that lines combining *ech2* and these mutations may be less likely to show altered phenotypes due to enzyme activity remaining at these steps. Taken together, these results suggest that active TAG hydrolysis and efficient fatty acid core β-oxidation are required for *ech2*-linked phenotypes.

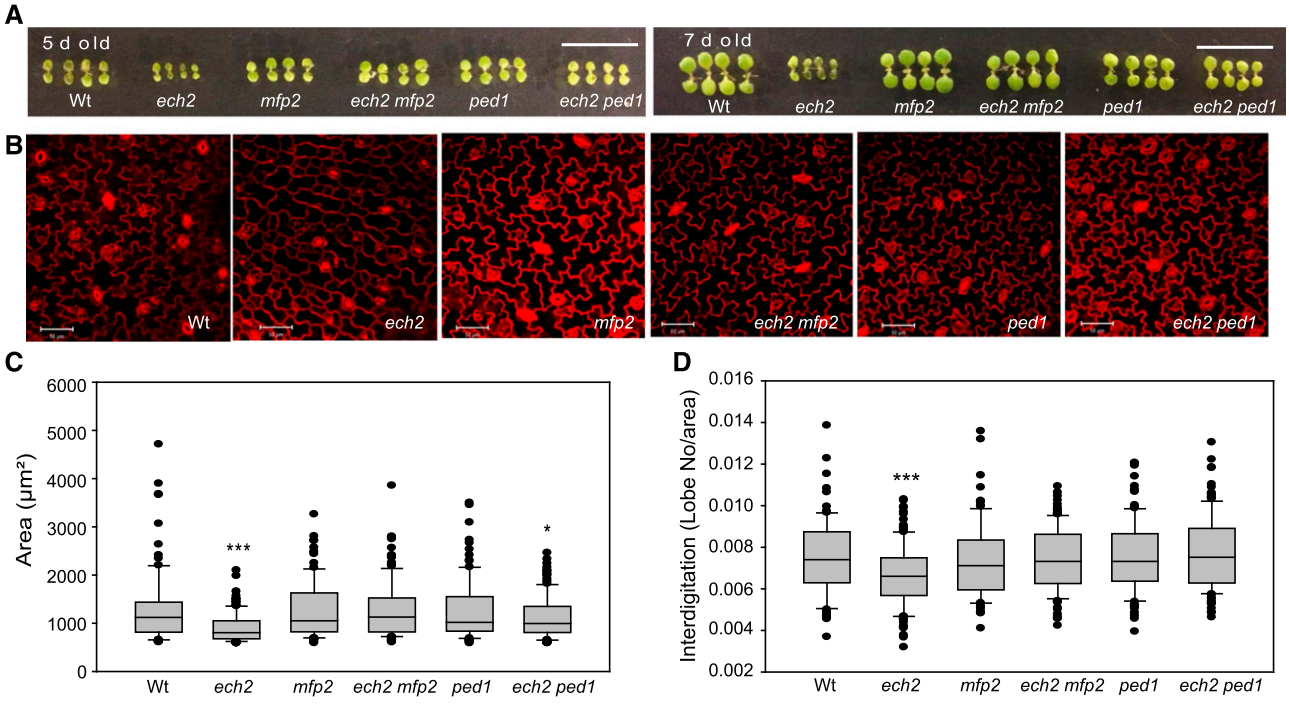

Figure 4. Either *mfp2* or *ped1* can suppress the deficiency of *ech2* in cell expansion. A, Cotyledons of wild type (Wt), *ech2*, *mfp2*, *ech2 mfp2*, *ped1*, and *ech2 ped1* seedlings 5 and 7 d after sowing. Bar = 1 cm. B, Confocal microscopy of propidium iodide-stained cotyledon pavement cells at d 5. Bar = 50 μm. C and D, The area (C) and interdigitation (D) of cotyledon pavement cell in 5-d-old seedlings (± SD; $n \geq 30$). *$P < 0.05$; ***$P < 0.005$ in Students' *t* test between wild type and mutants. Interdigitation, an index of interlocking levels between adjacent cells, was calculated by dividing lobe number by cell area.

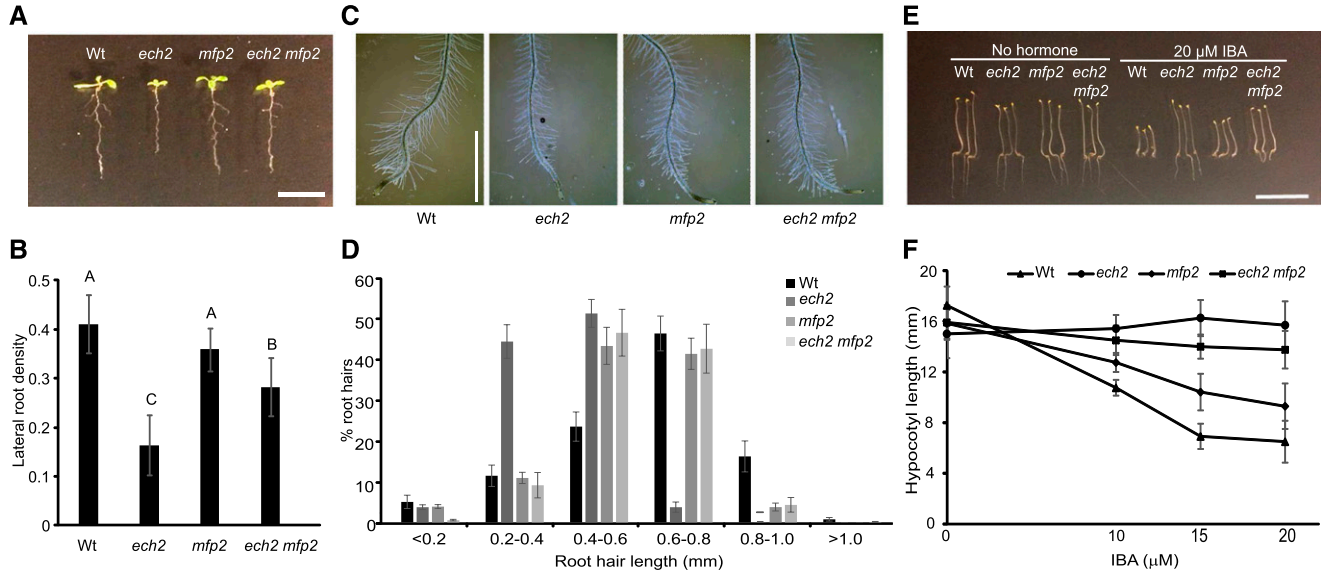

Figure 5. *mfp2* suppresses the deficiency of *ech2* in IBA to IAA conversion. A, 10-d-old wild-type (Wt), *ech2*, *mfp2*, and *ech2 mfp2* seedlings grown on medium with no hormone. Bar = 1 cm. B, Lateral root densities were calculated by dividing lateral root number by primary root length (SD ± ; $n \geq 10$). Statistical significance was determined by ANOVA and Tukey's multiple comparisons test ($P < 0.05$). Letters in common among the groups indicate no significant difference. C, Representative roots images of 7-d-old seedlings. Bar = 0.25 cm. D, Root hair length of 7-d-old seedlings was measured using ImageJ. Data are shown as a histogram of the percent of root hairs of each length range ± SD; $n \geq 10$. E, wild-type, *ech2*, *mfp2*, and *ech2 mfp2* seedlings grown 1 d in light, followed by 5 d in the dark on medium without hormone or with 20 μM IBA. Bar = 1 cm. F, Hypocotyl length of seedlings grown 1 d in light, followed by 5 d in the dark on media with 0, 10, 15, or 20 μM IBA. Data shown are ± SD; $n \geq 12$.

ech2 Over-Accumulates Short-Chain 3-Hydroxy Fatty Acids

The rescue of *ech2* phenotypic defects by addition of mutations disrupting TAG hydrolysis or core fatty acid β-oxidation suggests the accumulation of intermediates may be causing the defect in *ech2* cell expansion and resulting growth deficiencies. Based on the involvement of ECH2 activity in the catabolism of fatty acids with an even-numbered cis-double bond, potential candidates include (R)-3-hydroxy fatty acids.

To detect such compounds, we performed a direct scan of negatively charged lipid metabolites by ESI-MS. A unique peak ($m/z = -157.2$) was identified in *ech2* seedlings (Fig. 6). The m/z matches the $[M\text{-}H]^-$ ion of hydroxyoctenoic acid (C8:1 hydroxy fatty acid). To confirm the identity of the compound, gas chromatography –(GC)-MS was used to analyze the butyldimethylsilyl-derivatized lipid mixture, and the fragment fingerprint of each unique compound in *ech2* samples was analyzed. As expected, a unique peak was identified in the *ech2* sample (Supplemental Fig. S11). Analysis of the fragment fingerprint suggests the peak represents an 8-carbon fatty acid, with an ω-3 double bond and a 3-hydroxy group (Supplemental Fig. S11). Another peak of $m/z = -159.3$, which matches the $[M\text{-}H]^-$ ion of hydroxyoctanoic acid (C8:0 hydroxy fatty acid), was identified at a lower abundance (Fig. 6A). These short-chain 3-hydroxy fatty acids are likely the hydrolysis products of the corresponding β-oxidation acyl-CoA intermediates of ALA (C18:3) and linoleic acid (LA, C18:2), both of which have a double bond at the twelfth carbon requiring ECH2 for efficient degradation (Fig. 6B). Short-chain 3-hydroxy fatty acids were not detectable in *ech2* rosette leaves (Supplemental Fig. S12), and complementation lines had normal metabolism (Supplemental Fig. S2F), supporting our earlier finding that loss of ECH2 led to seedling-specific alterations.

The peak area in the ESI-MS scan was used to quantify the amount of these accumulated compounds. Although almost absent in wild type and *mfp2*, up to 20% of the total FFA pool was comprised of 3-hydroxyoctenoic acid and 3-hydroxyoctanoic acid in *ech2* (Fig. 6C). Interestingly, the *ech2 mfp2* double mutant accumulated much less 3-hydroxy fatty acids compared with *ech2* seedlings. As discussed before, MFP2 is one of the two primary enzymes that catalyze the core β-oxidation steps upstream of ECH2 for degradation of fatty acids with even-numbered cis-double bond (Fig. 1); its absence would severely limit the amount and rate of substrates supplied to ECH2. These results suggest the supply of substrate is kinetically important to the over-accumulation of the hydroxyoctenoic and hydroxyoctanoic acid products in *ech2* mutants.

Wild-type Seedlings Treated with 3-Hydroxyoctanoic Acid Show *ech2*-Like Responses in Many Different Aspects

The fatty acid metabolic analysis on *ech2* and *ech2 mfp2* suggests a connection between short-chain 3-hydroxy

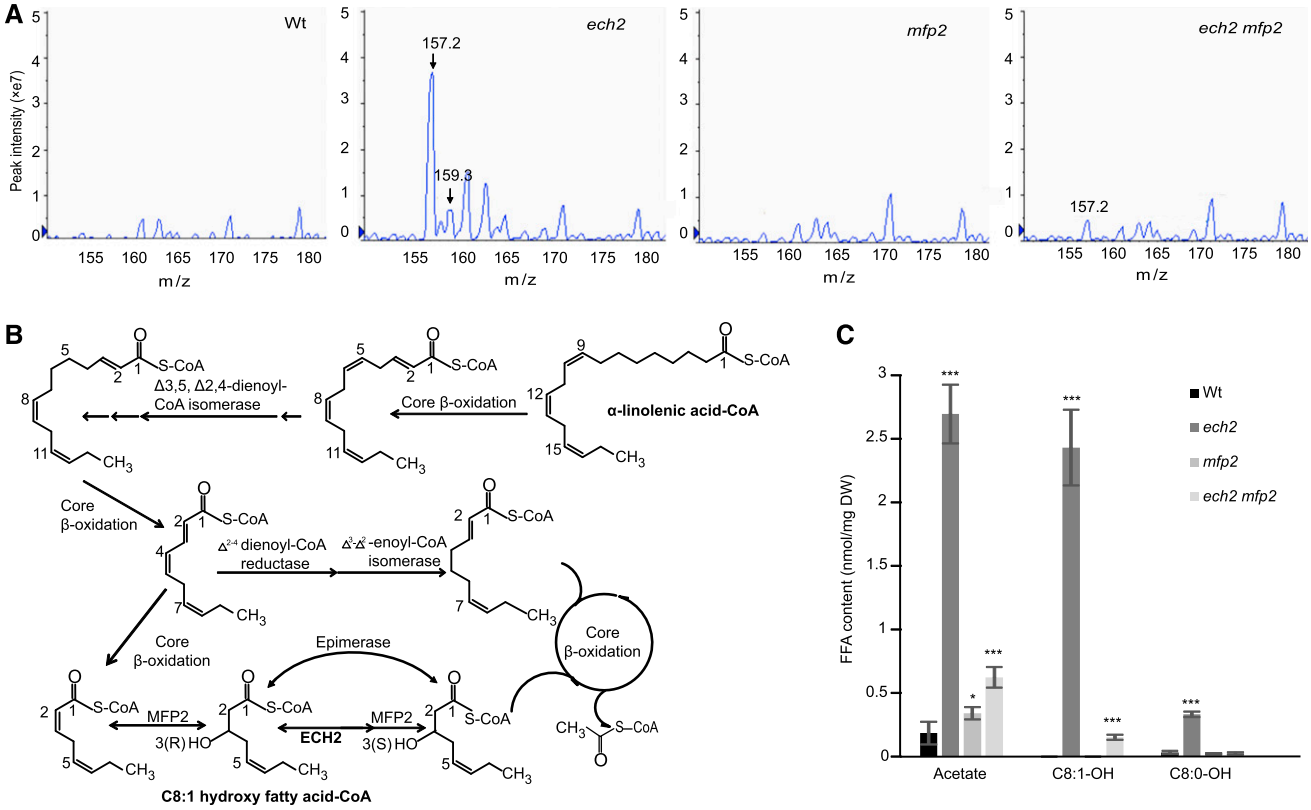

Figure 6. *ech2* over-accumulates short-chain 3-hydroxy fatty acids. A, ESI-MS spectra of lipid extracts of 3-d-old wild-type (Wt), *ech2*, *mfp2*, and *ech2 mfp2* seedlings. B, Putative β-oxidation of α-linolenic acid after the attachment of CoA. C8:1 hydroxy fatty acid-CoA is labeled as the substrate of ECH2. α-Linolenic acid also has cis double bonds at odd-numbered carbons (Δ9 and Δ15), and therefore complete degradation requires additional auxiliary enzyme activities including the Δ3,5, Δ2,4-dienoyl-CoA isomerase (DCI/Isomerase; Graham, 2008). Linoleic acid-CoA should be catabolized similarly despite the absent double bond at Δ15. C, Acetate, C8:1 hydroxy fatty acid (C8:1-OH), and C8:0 hydroxy fatty acid (C8:0-OH) content of 3-d-old wild-type, *ech2*, *mfp2*, and *ech2 mfp2* seedlings (± SD; $n = 5$). *$P < 0.05$; **$P < 0.01$; ***$P < 0.005$ in Student' *t* test between wild type and mutants.

fatty acid accumulation and *ech2* phenotypes. To test if there is a direct connection, wild-type seedlings treated with 3-hydroxyoctanoic acid were examined for seedling morphology, cotyledon pavement cell expansion, peroxisome morphology, and IBA response. Wild-type seedlings treated with 50 μM 3-hydroxyoctanoic acid had comparable root length and cotyledon area to mock-treated *ech2* seedlings (Fig. 7, A to D). 2-Hydroxyoctanoic acid was applied to test if the position of hydroxyl group affects the inhibitory effectiveness. A similar strong toxic effect was observed (Fig. 7A). However, when compared with 3-hydroxyoctanoic acid, 2-hydroxyoctanoic acid displayed a stronger inhibition effect on root elongation, but less inhibition on cotyledon expansion (Fig. 7, B to D). These results demonstrate that 3-hydroxyoctanoic acid treatment can cause *ech2*-like morphology alterations in wild-type seedlings, and fatty acids with hydroxy group at different positions have distinct effects on root and cotyledon development.

To further examine the effect of treatments on pavement cell patterning, pavement cells were imaged (Fig. 7E). Notably, pavement cells of wild-type seedlings treated with 3-hydroxyoctanoic acid showed reductions in both cell area and complexity, with similar levels to that of mock-treated *ech2*. (Fig. 7F). The same reductions were not detected in wild-type seedlings treated with 2-hydroxyoctanoic acid, even at applied concentrations sufficient to cause significantly reduced root elongation (Fig. 7B). These results indicate that treatment of 3-hydroxyoctanoic acid, but not 2-hydroxyoctanoic acid, can cause *ech2*-like defects in pavement cell development in wild-type seedlings.

To examine the effect of treatments on peroxisome morphology, wild-type and *ech2* seedlings expressing a peroxisomally targeted GFP were treated similarly. Peroxisomes in cotyledon pavement cells were imaged (A). As shown above, *ech2* seedlings had an increased peroxisome size and number compared with that of wild-type mock-treated seedlings (Supplemental Fig. S13, B and C). Significant gains in peroxisome size and number were observed in 3-hydroxyoctanoic acid–treated wild-type seedlings (Supplemental Fig. S13, B and C). 2-Hydroxyoctanoic acid–treated wild-type seedlings had mildly increased peroxisome size but

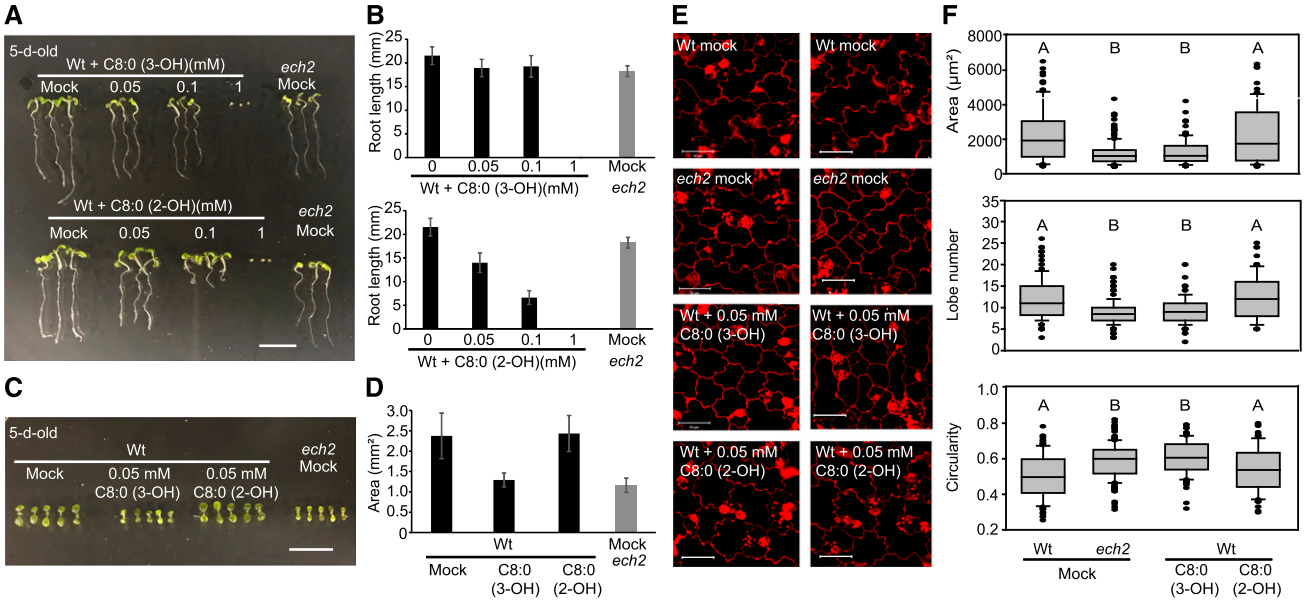

Figure 7. Wild-type (Wt) seedlings treated with 3-hydroxyoctanoic acid displayed defects on root and cotyledon development similar to *ech2*. A, 5-d-old wild-type seedlings treated with different concentrations of either 3-hydroxyoctanoic acid or 2-hydroxyoctanoic acid and mock-treated *ech2* seedlings. Bar = 1 cm. B, Root length of seedlings shown in (A) ± SD; $n > 10$. C and D, Cotyledon images (C) and cotyledon area (D) of 5-d-old wild-type seedlings treated with mock, 0.05 mM 3-hydroxyoctanoic acid, 0.05 mM 2-hydroxyoctanoic acid, and *ech2* seedlings treated with mock. Cotyledon area was measured with ImageJ, and averages are shown ± SD; $n > 10$. Bar = 1 cm. E, Representative confocal microscopy images of propidium iodide-stained cotyledon pavement cells of 6-d-old wild-type and *ech2* seedlings treated with mock, wild-type seedlings treated with 0.05 mM C8:0 (3-OH), and wild-type seedlings treated with 0.05 mM C8:0 (2-OH). Bar = 50 µm. F, The area (top), lobe number (middle), and circularity (bottom) of pavement cells. Data are shown ± SD; $n > 30$. Statistical significance was determined by ANOVA and Tukey's multiple comparisons test ($P < 0.05$). Letters in common among the groups indicate no significant difference.

comparable peroxisome number with that of mock-treated wild-type seedlings (Supplemental Fig. S13, B and C). These results suggest that 3-hydroxyoctanoic acid treatment can cause *ech2*-like defects in peroxisome morphology.

To test if the hydroxy fatty acid treatment can induce an altered IBA response in wild-type seedlings, root elongation and lateral root density were examined in wild-type seedlings grown in media with both hydroxyoctanoic acid and IBA. Wild-type seedlings showed increasing inhibition of root elongation with increasing IBA concentrations, whereas *ech2* showed IBA-resistant responses (Fig. 8, A and B). Intriguingly, wild-type seedlings treated with both 3-hydroxyoctanoic acid and IBA had reduced inhibition of root elongation compared with IBA treatment alone, indicating an *ech2*-like altered IBA response caused by the fatty acid treatment (Fig. 8B). Similarly, the effective concentration of IBA in lateral root stimulation was reduced by concurrent application of the fatty acid substrate (Fig. 8C). On the contrary, wild-type seedlings treated with 2-hydroxyoctanoic acid showed comparable root elongation and root branching to that of mock-treated wild-type seedlings under each IBA concentration (Fig. 8, B and C). Again, these results suggest that treatment of 3-hydroxyoctanoic acid, but not 2-hydroxyoctanoic acid, on wild-type seedlings can cause an altered IBA response similar to *ech2* seedlings.

ech2 Responds Differently to Treatments with Unsaturated Fatty Acid Depending on Bond Position

Considering the function of ECH2 in the degradation of unsaturated fatty acids on even-numbered carbon (Fig. 1; Goepfert et al., 2006), seedlings with low ECH2 activity are hypothesized to accumulate (R)-3-hydroxyacyl-CoA and/or associated hydrolyzed intermediates when treated with unsaturated fatty acids on even-numbered carbon, but not with unsaturated fatty acids on odd-numbered carbon. This differential metabolic accumulation may lead to different physiological responses. To test this hypothesis, wild-type and *ech2* seedlings were treated with Δ7-cis nonadecenoic acid (C19:1 Δ7-cis) and Δ10-cis nonadecenoic acid (C19:1 Δ10-cis). Root elongation of seedlings were tested. In both wild type and *ech2*, significant reductions of seedling root elongation were observed when treated with either substrate (Fig. 9). At this concentration, the reductions of root elongation in wild-type seedlings treated with either fatty acid were comparable. However, the inhibition of root elongation in *ech2* seedlings treated with Δ10-cis nonadecenoic acid was stronger

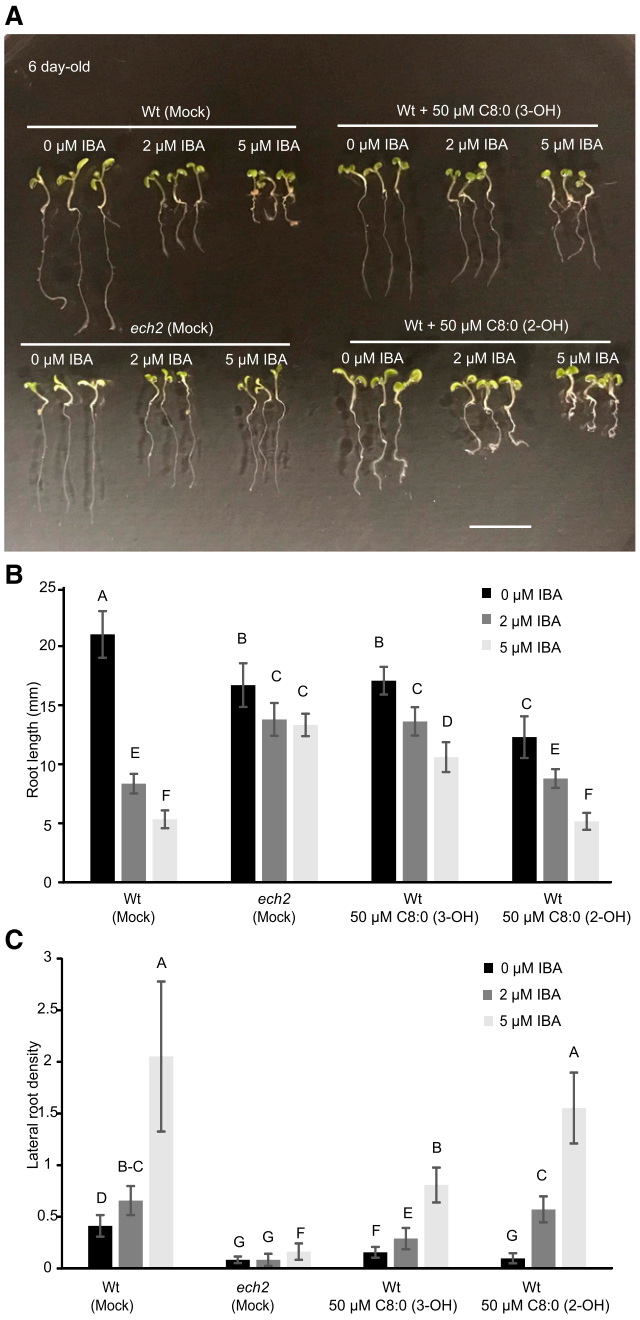

Figure 8. Wild-type (Wt) seedlings treated with 3-hydroxyoctanoic acid have *ech2*-like altered IBA response. A, Representative images of 6-d-old wild-type and *ech2* seedlings grown in media with different combinations of 3-hydroxyoctanoic acid (C8:0 3-OH), 2-hydroxyoctanoic acid (C8:0 2-OH), and IBA. Scale bar = 1 cm. B, Root length of seedlings shown in (A). C, Lateral root density of seedlings shown in (A). Data are shown ± SD; $n > 10$. Statistical significance was determined by ANOVA and Tukey's multiple comparisons test ($P < 0.05$). Letters in common among the groups indicate no significant difference.

compared with *ech2* seedlings treated with Δ7-cis nonadecenoic acid (Fig. 9). These results show that wild-type seedlings are equally inhibited by Δ10-cis nonadecenoic acid and Δ7-cis nonadecenoic acid treatments; *ech2* seedlings are more sensitive to Δ10-cis nonadecenoic acid than Δ7-cis nonadecenoic acid treatment.

DISCUSSION

Peroxisomes are important organelles that harbor lipophilic pathways required for plant growth, development, and responses to changing environmental conditions. Fatty acid catabolism and IBA to IAA conversion are peroxisomal pathways that occur via similar β-oxidation mechanisms. Mutants exclusively defective in IBA to IAA conversion were defined by their aberrant responses to IBA; exogenous Suc is not required for their seedling establishment, ruling out alterations in fatty acid metabolism. However, other mutants have disruptions in both IBA-response pathways and fatty acid metabolism. These mutations typically fall into two classes: mutations disrupting overall peroxisome import or activity and those in enzymes with a primary function in fatty acid β-oxidation that also impact IBA metabolism (Hu et al., 2012). Here, we focused on *ech2*, which has defects in both peroxisomal pathways while also having unique early growth defect.

ech2 Has Unique Growth and Metabolic Phenotypes

The *ech2-1* mutant, referred to here as *ech2*, was identified in a screen for mutants with altered IBA response (Strader et al., 2011). The study demonstrated the requirement of IBA-derived IAA in Arabidopsis seedling development by characterizing phenotypes of the quadruple mutant *ibr1ibr3ibr10ech2*. The strong IBA resistance displayed in this line suggested reductions in IBA to IAA conversion (Strader et al., 2011). Moreover, the altered IBA response of *ech2* was rescued in transgenic lines carrying *35S:HA-ECH2*. Here, we further characterized the *ech2* mutant in seedling morphology, and found that *ech2* alone has reduced cotyledon expansion and short root length as seen in *ibr1ibr3ibr10ech2* (Fig. 2; Strader et al., 2010). A similar reduced cotyledon expansion phenotype was observed in *ech2-2* (Katano et al., 2016). To confirm these phenotypes results from the loss of ECH2 function, a *35S:ECH2* construct was transformed into the *ech2* background. Homozygous *ech2(ECH2)* transgenic lines had normal growth responses in phenotypic assays, including both the seedling development and metabolic phenotypes (Supplemental Fig. S2). Notably, studies of an *ECH2* RNAi line showed a wild-type physical appearance and normal responses to the IBA analog 2,4-dichlorophenoxybutyric acid (Goepfert et al., 2006). These discrepancies suggest that ECH2 activity is more reduced in the *ech2* mutant than in the *ECH2* RNAi line (Goepfert et al., 2006; Strader et., 2010). Therefore, we focused on expanding studies of the role of ECH2 using the *ech2-1* mutant and an *ech2(ECH2)* complementation line.

ech2 phenotypes are related to alterations reported in two peroxisomal pathways: fatty acid β-oxidation and IBA to IAA conversion. *ech2* cotyledons have retarded oil body mobilization and enlarged peroxisomes (Fig. 3), similar to other mutants with impaired fatty acid metabolism (Rinaldi et al., 2016). The root growth defect of *ech2* is alleviated on media with Suc (Supplemental Fig. S6), similar to fatty acid catabolism mutants including *sdp1* and *mfp2* (Supplemental Fig. S14; Thazar-Poulot et al., 2015). *ech2* also is resistant to exogenous IBA application (Fig. 5) and has small cotyledons and short root hairs (Figs. 2 and 5), similar to the triple IBA-response mutant *ibr1 ibr3 ibr10* (Strader et al., 2010). These mutant phenotypes suggest the ECH2 enzyme affects both fatty acid catabolism and IBA to IAA conversion.

However, the compromised fatty acid metabolism of *ech2* is distinct from that of *mfp2* and *ped1*. *ech2* peroxisomes are larger than in wild type (Fig. 3), but smaller than in *mfp2* and *ped1* (Rinaldi et al., 2016). Also, the increased peroxisome numbers in *ech2* (Fig. 3) have not been reported in either *mfp2* or *ped1*. When compared with that in *mfp2* and *ped1*, reductions in hypocotyl elongation of dark-grown *ech2* are minor and not rescued by Suc (Supplemental Fig. S7). These distinctions suggest *ech2* disrupts fatty acid metabolism to only a mild degree. Further, auxin did not restore root hair elongation to the level of wild type (Supplemental Fig. S15). Both *ech2* and wild-type root hairs elongate with auxin treatment. Unlike *ibr1 ibr3 ibr10*, which has short root hairs that recover to lengths similar to wild type following auxin application (Strader et al., 2010), the differential between wild type and *ech2* remains consistent plus or minus auxin, suggesting the additional auxin does not overcome or is not the primary cause of inhibited root hair elongation. Finally, the *ech2* small cotyledon phenotype is not rescued by exogenous sugar or auxin (Supplemental Figs. S5 and S6). These observations led us to consider potential underlying mechanisms other than the reduced production of energy/short-chain carbons or IBA-derived auxin.

Alternatively, *ech2* responses could be due to decreased production of a particular product or indirect effects resulting from reduced intermediates required for a secondary pathway or accumulation of substrates or intermediates with potentially toxic consequences. We investigated the hypothesis that *ech2* phenotypes result from the toxic accumulation of molecules that normally require ECH2 activity to be effectively metabolized. A previous report described a feeding experiment in which *ECH2* RNAi lines expressing a polyhydroxyalkanoate (PHA) synthase were incubated with even cis-unsaturated fatty acids. Accumulation of PHA9:0 produced from corresponding 3-hydroxyacyl-CoAs (C9:0-OH) was observed, suggesting ECH2 is required to metabolize (R)-3-hydroxyacyl-CoAs (Goepfert et al., 2006). Arabidopsis seeds accumulate large amounts of polyunsaturated fatty acids, primarily LA and ALA, which contain even cis-double bonds at the Δ12 carbon (O'Neill et al., 2003).

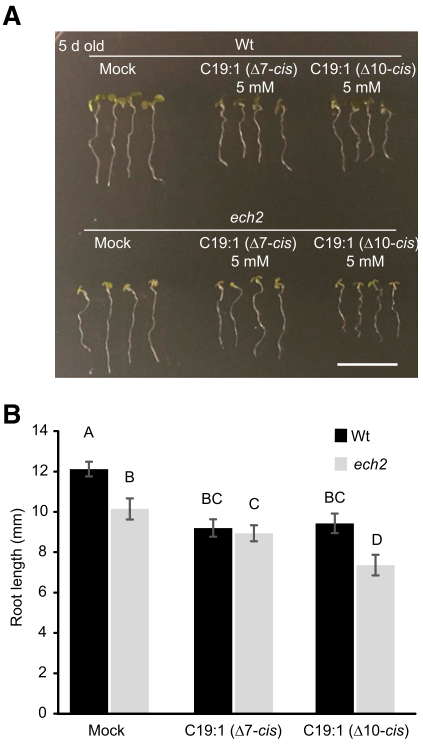

Figure 9. Δ7-Cis nonadecenoic acid treatment and Δ10-cis nonadecenoic acid treatment inhibit root elongation of *ech2* seedlings to different levels. A, 5-d-old wild-type (Wt; top) and *ech2* (bottom) seedlings treated with mock, 5 mM Δ7-cis nonadecenoic acid (C19:1 [Δ7-cis]), or 5 mM Δ10-cis nonadecenoic acid (C19:1 [Δ10-cis]). Scale bar = 1 cm. B, Root length of seedlings shown in (A) ± SE; $n > 10$. Statistical significance was determined by ANOVA and Tukey's multiple comparisons test ($P < 0.05$). Letters in common among the groups indicate no significant difference.

ECH2 RNAi lines also over-accumulated PHA8:0 and PHA8:1, corresponding to the metabolic intermediates of endogenous LA and ALA (Goepfert et al., 2006). Although these results are consistent with our toxic intermediate hypothesis, intermediate accumulation levels under normal background may not result from the accumulation of PHA. Additionally, the accumulation of a new product can have broader impacts to the metabolic and/or signaling network in cells and the consequences of such accumulation need to be examined in the context of plant morphology and development.

To explore *ech2* metabolic changes, we profiled the fatty acid spectrum in wild type and mutants. We detected 3-hydroxyoctanoic acid (C8:0-OH) and 3-hydroxyoctenoic acid (C8:1-OH) accumulation in *ech2* (Fig. 6). C8:1-OH levels are ~ 7-fold higher than C8:0-OH (Fig. 6C). This pattern is opposite to the ALA and LA distribution in Arabidopsis seeds, which typically have 21% ALA and 33% LA (O'Neill et al., 2003). It is possible that ALA is metabolized to a higher degree than LA due to unknown enzyme specificities, C8:0-OH-CoA could be further metabolized by alternative pathways, or acyl-CoA thioesterases prefer C8:1-OH-CoA for hydrolysis.

In addition to the accumulation of these intermediates directly related to ECH2 loss, we also found an accumulation of acetate (Fig. 6C). The lack of other FFAs (Supplemental Table S1) suggests the stall happens specifically, whereas the overall functionality of β-oxidation is less affected. Our in vitro β-oxidation assay show *ech2* also has reduced enoyl-CoA hydratase 1 activity, but in a minor way compared with *mfp2* (Supplemental Fig. S8; Rylott et al., 2006). The decreased enoyl-CoA hydratase 1 activity in *ech2* may be an indirect inhibitory effect of accumulated abnormal FFAs, as previous reports suggest ECH2 only possesses enoyl-CoA hydratase 2 activity (Goepfert et al., 2006). The functional core β-oxidation precludes the complete disruption of fatty acid catabolism that might result from loss of ECH2.

Efficient Substrate Supply is Required for the Accumulation of Fatty Acid Intermediates and Resulting Phenotypes in *ech2*-Containing Mutants

We did epistatic analysis to investigate the genetic interactions between *ech2* and other mutants defective in peroxisomal enzymes. Our results showed that *ibr* higher-order mutants containing *ech2* displayed similar growth phenotypes to *ech2* (Supplemental Fig. S9A), consistent with previous results describing *ibr1 ibr3 ibr10 ech2* (Strader et al., 2011). However, mutants disrupting enzymes upstream of ECH2 in fatty acid metabolic pathways suppress the *ech2* growth phenotypes, including *mfp2*, *ped1*, and *sdp1*. The fatty acid catabolism defects determine the severity of the growth defects in *ech2*-containing mutant combinations. In the catabolism of even cis-unsaturated fatty acids, SDP1, MFP2, and PED1 catalyze the steps preceding ECH2 activity to generate (R)-3-hydroxyacyl-CoAs (Fig. 1). ECH2 disruption would disrupt the substrate-product balance, resulting in accumulation of (R)-3-hydroxyacyl-CoAs. If this step is stalled for a prolonged period, these intermediates could build up or be degraded to recycle CoA and produce free (R)-3-hydroxy fatty acids. Concurrent reductions of an upstream enzyme and ECH2 reduce the supply of these substrates and minimize accumulation of (R)-3-hydroxy fatty acids, thus restoring the metabolic balance and reducing the phenotypic severity. Free fatty acid profiles of wild type and mutant lines support this hypothesis. In *ech2 mfp2*, accumulation of short-chain hydroxy fatty acids and acetate were suppressed compared with *ech2* (Fig. 6; Supplemental Table S1).

The *ech2* FFA profile also suggests the importance of the hydratase/epimerase pathway to degrade fatty acids with an even-numbered cis-double bond. Previous results demonstrated the alterative reductase/isomerase pathway (Fig. 1) contributes to FFA degradation (Allenbach and Poirier, 2000). However, the dramatic 3-hydroxy-5-octenoic acid accumulation in *ech2* (~ 20% of total FFA pool; Fig. 6C) leads to questions about activity of the reductase/isomerase pathway. The production of the ECH2 substrate requires one round of core β-oxidation of the 2-trans-4-cis-dienoyl-CoA intermediate and hydration by MFP2; these steps are not reversible (Fig. 1; Graham, 2008), and therefore accumulating intermediates cannot be degraded by the reductase/isomerase pathway. Auxiliary enzymes, including 3-hydroxyacyl-CoA epimerase, DECR, and Δ3, Δ2-enoyl-CoA isomerases (AtECI), are not well studied, and future mutant analysis and metabolic profiling are necessary to understand the activation of and biological importance for the reductase/isomerase pathway.

Accumulation of Fatty Acid Intermediates Affects Auxin Metabolism

The IBA-response mutant *ibr1 ibr3 ibr10 ech2* has an ~20% reduction in IAA levels, indicating IBA conversion is a major contributor to the auxin pool (Strader et al., 2011). One of the most surprising observations in this study is the restoration of IBA sensitivity when *ech2* was crossed with fatty acid catabolism mutants. Previous studies hypothesized ECH2 as a shared enoyl-CoA hydratase acting in both fatty acid catabolism and IBA to IAA conversion (Goepfert et al., 2006; Strader et al., 2011). If the overlap between these two peroxisomal pathways happens at the catalytic level, we would hypothesize combination mutants to have unchanged or enhanced IBA resistance, as the additional fatty acid catabolism mutant would also negatively affect IBA to IAA conversion. This opposite observation led us to hypothesize other effects resulting from loss of *ECH2* that affect these pathways (Fig. 5).

We also uncovered an association between short-chain 3-hydroxy fatty acids and IBA resistance in *ech2*-containing mutants. Consistently, treatment of 3-hydroxyoctanoic acid on wild-type seedlings caused an altered IBA response similar to that of *ech2* seedlings (Fig. 8). The accumulation in the mutant or feeding in the wild-type seedlings could be due to direct disruption of peroxisomal IBA pathways. The unexpected over-accumulation of free acetate in *ech2* (Fig. 6C) led to a second potential hypothesis. Unlike long-chain and very long-chain acyl-CoAs, acetyl-CoA is the β-oxidation end product. Increased conversion of acetyl CoA to acetate is not likely the result of a direct feedback effect of elevated intermediates. Instead, it may reflect the increased need for local or global CoA recycling as a result of stalled (R)-3-hydroxy acyl-CoA in *ech2*. A similar effect could affect the co-localized IBA(-CoA) to IAA(-CoA) pathway, decreasing its efficiency and causing the IBA resistance phenotype. CoA limitations have been suggested previously to affect IBA metabolism in mutants disrupting the ACX proteins required for β-oxidation as well (Adham et al., 2005). It is necessary to study these genetic, metabolic, and regulatory interactions systematically, to understand the full picture of peroxisome function in the context of auxin homeostasis and its influence on early plant development.

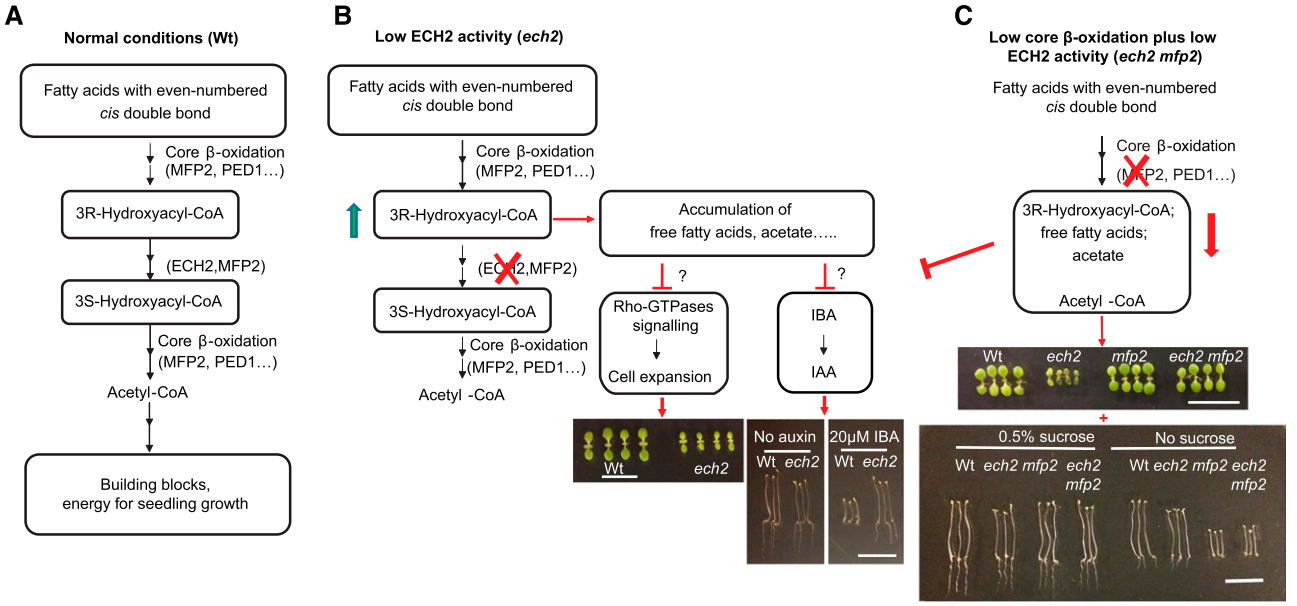

Figure 10. Schematic model of how low ECH2 activity alters metabolic pathways that influence fatty acid catabolism and IBA to IAA conversion during seedling development in *Arabidopsis thaliana*. A, ECH2 functions in the hydratase pathway for the degradation of unsaturated fatty acids with a cis-double bond on an even-numbered carbon. B, Low ECH2 activity, indicated in this study by an *ech2* mutant, results in accumulation of short-chain 3-hydroxyacyl acids and acetate, which suppress IBA to IAA conversion and cotyledon cell expansion via Rho GTPase signaling and other undetermined pathways. C, *Ech2 mfp2* displays phenotypes similar to *mfp2*. Low ECH2 activity has less impact on a cell when core β-oxidation pathway activity also is reduced. In the *ech2* background, MFP2 dysfunction results in the reduced production of acetyl-CoA, ECH2 substrates, and associated metabolites, releasing the suppression on cell expansion and IBA to IAA conversion. Exogenous Suc still is required for seedling establishment in *mfp2* and *ech2 mfp2* due to the reduced energy production when β-oxidation pathways are not active. For all panels, bar = 1 cm.

Position of Hydroxyl Group and Double Bond Affect the Inhibitory Specificity and Potency of FFAs

3-Hydroxyoctanoic acid treated wild-type seedlings phenocopied *ech2* (Figs. 7 and 8; Supplemental Fig. S14). Treatment with 2-hydroxyoctanoic acid resulted in similar root defects but milder cotyledon defects than *ech2* (Fig. 7). The different structures of the two hydroxyoctanoic acids may make them effective against different targets, as 2-hydroxyoctanoate inhibits medium chain acyl-CoA synthetase in mammals (Kasuya et al., 1996), while we hypothesize 3-hydroxyoctanoate would competitively inhibit/saturate enoyl-CoA hydratases. It is plausible the competitive inhibition can happen on acetyl-CoA synthetases in Arabidopsis, the closest homologs of mammalian medium chain acyl-CoA synthetase, by both 2- and 3-hydroxyoctanoate, and other FFAs at higher concentrations. The additional inhibitory effect of 3-hydroxyoctanoic acid may contribute more to the cotyledon defect with the overlapping effects on peroxisomal β-oxidation pathways.

Application of FFAs has general adverse effects on plant growth (Li et al., 2011; Fan et al., 2013). To distinguish the general inhibition effect from defects specific to the loss of ECH2, it is beneficial to study the positional effect of double bond on the specificity and potency of the applied FFA to wild type and *ech2*. We compared the inhibitory effect of two nonadecenoic acids (C19:1, cis-Δ7, and cis-Δ10) and found they differentially inhibited the growth of wild type and *ech2* (Fig. 9). Notably, wild type showed no significant difference under the effect of either C19:1, displaying only the general FFA toxicity effect. In contrast, *ech2* was further inhibited by C19:1-cis-Δ10 but not by C19:1-cis-Δ7. This experiment further strengthens the importance of ECH2 to the proper degradation of even cis-double bond FFAs.

Perspectives

We have investigated the metabolic alterations underlying the *ech2* phenotypes. Loss of ECH2 led to aberrant accumulation of intermediates from fatty acid catabolism pathways, resulting in seedling growth defects. A metabolic shift following the simultaneous loss of MFP2 reduced the growth defects of *ech2*. We also have gained insights into potential interactions between peroxisomal pathways. *ech2* accumulates FFA intermediates that are not present under normal conditions, resulting in exaggerated phenotypic responses. From this information, we can make valuable inferences and form new hypotheses about the roles of FFAs in metabolic crosstalk and potential signaling between peroxisomal pathways.

Our results and current hypotheses are illustrated in Figure 10. 3-Hydroxy fatty acids accumulate when ECH2 levels are low, as exemplified in this work by the *ech2* mutant. In turn, this metabolic defect reduces IBA to IAA conversion and impacts epidermal cell expansion, possibly through the ROP pathway. At the cellular level, these metabolic changes lead to reduced oil body mobilization and increases in peroxisome number and size. Simultaneous reduction of core β-oxidation pathways, as exemplified by the double mutants in our studies, reduce the need for ECH2 activity because a decreased amount of substrate is available for metabolism. Future studies, including the direct profiling of IBA to IAA conversion intermediates and cell-specific testing of upstream effectors and downstream signaling components of the ROP pathway, may reveal additional components of and connections between these metabolic and signaling pathways.

Better understanding the mechanism underlying FFA lipotoxicity, especially of hydroxy fatty acids, also has great benefits for industrial purposes. Hydroxy fatty acids are frequently used as additives or raw materials for chemical feedstocks, lubricants, inks, and plastics (Lee et al., 2015). Metabolic engineering approaches have been used to produce hydroxy fatty acids in Arabidopsis seeds. However, transgenic plants successfully producing such compounds have low seed oil and poor seedling establishment, similar to *ech2* (Lunn et al., 2018). Further studies of the potential downstream processes of FFA signaling as well as transcriptome and proteome changes in *ech2* and FFA treated plants will greatly improve our understanding of peroxisomal lipid metabolism and regulation in seeds and developing plants.

MATERIALS AND METHODS

Plant Materials

Arabidopsis (*Arabidopsis thaliana*) mutants are in the Colombia (Col-0) background. *Ech2-1* has a G-A mutation in At1g76150 (Gly-36-to-Glu substitution) and was originally isolated as IBA resistant in hypocotyl growth (Strader et al., 2011). *Ibr1-2, ibr3-1*, and *ped1-96* are ethyl methanesulfonate-based point mutations that have been described previously (Zolman et al., 2000, 2007, 2008; Lingard and Bartel, 2009). *Ibr10-1* contains a large in frame deletion in At4g14430 (Zolman et al., 2008). Insertion mutants include *acx3-6* (SALK_044956; Adham et al., 2005), *mfp2-2* (SALK_098016C; Rylott et al., 2006), *aim1-1* (SALK_023469; Richmond and Bleecker, 1999), and *sdp1* (SALK_102887; Eastmond, 2006; Thazar-Poulot et al., 2015). All mutants were crossed with *ech2-1* to generate higher-order mutants for assays. A *p35S: PTS2-GFP* (Woodward and Bartel, 2005) wild-type line was crossed into mutant lines to examine peroxisome morphology.

Plant Growth and Phenotypic Assays

Seeds were surface-sterilized and imbibed at 4°C in darkness for 3 to 4 d, and then plated on plant nutrient (PN) medium (Haughn and Somerville, 1986) solidified with 0.6% (w/v) agar. Then 0.5% (w/v) Suc was added (PNS) when indicated. Plates were incubated at 22°C in continuous light. Seedlings were used for phenotypic assays, transferred to soil, and grown at 18–22°C in long-day conditions (16 h light, 8 h darkness).

To measure cotyledon area, seedlings were grown on PNS under white light for 7 d. Cotyledons were imaged by confocal microscopy, and the area was measured using National Institutes of Health (NIH) Image software (https://imagej.nih.gov/ij/). To examine root elongation, seedlings were grown for 7-9 d and removed from the agar to measure the primary root length.

To examine the effect of Suc on seedling establishment, seeds were plated on PN or PNS medium for 7 d, and then the cotyledon area and root length were measured. For dark grown seedlings, seeds were plated on PN or on PNS medium for 1 d under white light, and then transferred to dark for an additional 5 d growth. Hypocotyl lengths were measured.

To examine the effect of auxin on cotyledon pavement cells expansion, surface sterilized seeds were germinated in liquid half strength Murashige and Skoog medium (Toshio and Folke, 1962) with the indicated concentration of Naphthalene-1-acetic acid (GoldBio; Xu et al., 2010). Cotyledons were detached, and pavement cells were imaged at 3 d.

To measure root hair length, seedlings were grown at 22°C in continuous light for 7 d on PNS or PNS with indicated concentration of auxin. When auxin was added, plates were incubated under yellow filters to protect indolic compound from breakdown (Stasinopoulos and Hangarter, 1990). Seedlings were removed and immersed in 5% (v/v) glycerol. Root hairs were imaged using an EVOS Floid cell Imaging Station and measured using NIH Image software.

To examine IBA response, surface sterilized seeds were plated on PNS or PNS with indicated concentrations of IBA (GoldBio) for 1 d under light with yellow filters, and then transferred to dark for an additional 5 d growth. Hypocotyl lengths were measured. For root elongation assays, surface sterilized seeds were plated on media for 7 d under light with yellow filters. Root lengths were then measured.

Statistical analysis was completed for each assay as indicated using GraphPad Prism.

Vector Construction and Plant Transformation

For complementation of the *ech2* mutant, ECH2 and HA tag coding sequence were amplified from the pEarleyGate 201 plasmid containing a N-terminal HA-fusion ECH2 (Strader et al., 2011). PCR products were digested and inserted into 35SFAST plant expression vector (Ge et al., 2005), replacing the Flag/Strep tag within the multiple cloning sites *Bam*HI and *Sal*I.

35S-*HA-ECH2* was introduced into *Agrobacterium tumefaciens* GV3101 (Koncz and Schell, 1986) and transformed into *ech2* using the floral dip method (Clough and Bent, 1998). Transformants were selected on media supplemented with 25 μg/mL Kanamycin and verified with genomic PCR.

Confocal Microscopy and Organelle Quantification

Seedlings were submerged in propidium iodide (10 μg/mL; Molecular Probes) for at least 10 min to label cell walls. Adaxial cotyledon pavement cells were imaged using a Zeiss LSM 700 laser scanning confocal microscope with a 20× or 63× lens. Area and circularity [4(area/perimeter^2)] of each cell were determined using NIH Image software. Number of lobes was automatically counted by Lobefinder software (Wu et al., 2016) and the PaCeQuant plugin in NIH Image software (Möller et al., 2017). Lobes were manually counted for confirmation.

For Nile red staining, seedlings were submerged in 5 μg/ml Nile red for at least 10 min. Cotyledon oil bodies were imaged under confocal microscope through a 63× oil immersion lens. The same lens was used to detect GFP signals to image the peroxisomes in seedlings with *p35S: PTS2-GFP* background. Samples was excited with a 488-nm laser line, and fluorescence emission was collected for best signals of indicated fluorescent probes.

For each 202.5 × 202.5 μm confocal image, fluorescence area and organelle number was measured using NIH Image software. Images were converted to 8-bit binary images. The Threshold tool was used to designate objects (oil bodies or peroxisomes) with manual settings. Fluorescence area and objects number were measured by the Analyze Particles function.

Fatty Acid β-Oxidation Assays

After surface sterilization, seeds were plated on PNS medium covered with filter paper. β-Oxidation assays were performed according to Rylott et al., 2006. Briefly, total proteins were extracted and desalted by disposable PD MidiTrap G-10 columns (GE Healthcare) using the centrifugation protocol. Each assay was initiated by adding acyl-CoA substrate to the reaction mix containing desalted protein. The relative abundance of acyl-CoA, enoyl-CoA, hydroxyacyl-CoA, ketoacyl-CoA in the β-oxidation series was determined by an ESI-MS/MS based method adapted from Rylott et al., 2006.

RNA Extraction and Expression Analysis

Seedlings or rosette leaves were collected at the indicated time and homogenized in liquid nitrogen. RNA was extracted using the IBI Mini Total RNA Kit (Plant; MidSci). Expression levels of genes of interest were determined and normalized to that of Ubiquitin10 (At4G05320) with the BioRad CFX96 Real Time PCR System using Bullseye EvaGreen quantitative PCR Mix (MidSci). No reverse transcriptase and no complementary DNA (cDNA) reactions were used as negative controls. Primers for each gene are listed in Supplemental Table S2. Experiments were performed with both biological and technical triplicates.

Feeding Experiments

Surface-sterilized seeds were placed at 4°C for 72 h, and then transferred to liquid PN containing 0.5% (w/v) Suc, 2% (w/v) pluronic-127 (Millipore Sigma), and fatty acids at the indicated concentration. Constant light and agitation (70 rpm) were applied. 2-Hydroxyoctanoic acid was purchased from Millipore Sigma; 3-hydroxyoctanoic acid was purchased from Matreya LLC (www.Matreya.com). Δ7-Cis nonadecenoic acid and Δ10-cis nonadecenoic acid were purchased from NU-CHEK-PREP, INC (www.nu-chekprep.com).

Lipid Extraction

Total lipid extraction was performed according to method of Liu and Wang, 2016. Briefly, fresh tissues (3-d-old seedlings or 21-d rosette leaves) were incubated in preheated (75°C) isopropanol for 15 min to inactivate phospholipase D activity (Liu et al., 2015). Up to five extractions using lipid extraction solution (Chloroform: methanol = 2:1 [v/v]) were performed. All the extracts were collected, and lipids phases were washed with 1 M KCl and water sequentially. Lipids were dried under nitrogen evaporator, and then diluted with methanol for downstream analysis.

Analysis of Free Fatty Acids by ESI-MS and Gas Chromatography–Mass Spectrometry

FFAs in extracted lipid samples were analyzed directly by ESI-MS. The scanning method was adapted from Li et al., 2011 with slight modification. Briefly, lipid samples were scanned in negative ion mode (−4500kV, −Q1) between 50 and 400 D on API 4000 mass spectrometry. Heptadecanoic acid (17:0) was used as internal standard. Acquired data were subjected to background subtraction and normalization to internal standard and dry weight of plant material. Five biological repeats were used for each genotype and treatment.

Agilent 5975C GC/MSD system was used to characterize new fatty acid intermediates. Lipid samples were hydrolyzed by 0.5 M HCl in acetonitrile/water (9:1) at 100°C for 1 h, followed by chloroform extraction. The organic phase was pooled and dried under nitrogen gas, and the derivatization was performed by adding 50 μL *N-tert*-Butyldimethylsilyl-*N*-methyltrifluoroacetamide (with 1% [w/v] *tert*-Butyldimethylchlorosilane) and 50 μL N,*N*-dimethylformamide and incubating at 70°C for 1 h. Samples were separated by J&W DB-5ms capillary column (Agilent, 122-5562G), from 80°C to 310°C with a ramping rate at 20°C/min. MSD scan range was set to 50–550 D. Unique peaks in *ech2* samples but not wild type were individually checked. Each significant unique ion was mapped to potential fragments from pseudo-molecular ions due to the instability of the theoretical molecular ion of the double derivatized 3-hydroxyoctenoic acid. The retention time was also considered. An alternative derivatization method using methylation followed by silylation was used to further confirm the results.

Accession Numbers

Sequence data from this article can be found in the EMBL/GenBank database or the Arabidopsis Genome Initiative database under the following accession numbers: *ECH2*, AT1G76150; *IBR1*, AT4G05530; *IBR3*, AT3G06810; *IBR10*, AT4G14430; *MFP2*, AT3G06860; *AIM1*, AT4G29010; *ACX3*, AT1G06290; *PED1*, AT2G33150; *SDP1*, AT5G04040; *ROP2*, At1g20090; *ROP4*, At1g75840; *ROP6*, At1g10840; *RIC1*, At2g33460; *RIC4*, At5g16490.

Supplemental Data

The following supplemental materials are available.

Supplemental Figure S1. Only *ech2* shows reduced cotyledon size and primary root length.

Supplemental Figure S2. *ech2* is rescued by *ECH2*.

Supplemental Figure S3. Dry seed weight and germination rate of *ech2* seeds are comparable to those of Wt.

Supplemental Figure S4. *ech2* cotyledons have reduced *ROP* expression levels.

Supplemental Figure S5. Auxin application is not able to improve pavement cell expansion in *ech2* cotyledons.

Supplemental Figure S6. *ech2* displays better seedling growth on Suc-containing medium than on medium with no Suc.

Supplemental Figure S7. *ech2* shows similar elongation reductions in dark-grown hypocotyl regardless of the absence or presence of Suc.

Supplemental Figure S8. Enoyl-CoA hydratase activity on acyl-CoA oxidase product is disrupted in *ech2* seedlings.

Supplemental Figure S9. Either *mfp2* or *ped1* can suppress the defects of *ech2* in cotyledon development regardless of the conversion levels of IBA to IAA.

Supplemental Figure S10. Efficient TAG hydrolysis and fatty acid core β-oxidation are required for *ech2* phenotypes.

Supplemental Figure S11. GC-MS is used to confirm the identification of the unique peak in *ech2* samples.

Supplemental Figure S12. C8:1 hydroxy fatty acid (*m/z* = -157) and C8:0 hydroxy fatty acid (*m/z* = -159) are not accumulated in rosette leaves.

Supplemental Figure S13. 3-Hydroxyoctanoic acid treatment affects peroxisome size and number.

Supplemental Figure S14. Suc application improves seedling establishment of light-grown *mfp2* and *ech2 mfp2*.

Supplemental Figure S15. Application of auxin does not restore root hair elongation defects in *ech2*.

Supplemental Table S1. FFA content of 3-d-old Wt, *ech2*, *mfp2*, and *ech2 mfp2* seedlings.

Supplemental Table S2. Primers used for qPCR.

ACKNOWLEDGMENTS

We thank the Arabidopsis Biological Resource Center at Ohio State University for seed stocks and the Salk Institute Genomic Analysis Laboratory for generating the sequence-indexed Arabidopsis T-DNA insertion mutants. We appreciate the gifts of *ech2-1* seeds and *p35S: HA-ECH2* plasmid from Lucia Strader, and *ped1-96* and *p35S: PTS2-GFP* wild-type seeds from Bonnie Bartel. We gratefully acknowledge members of the Zolman lab for assistance generating plant lines and Vanessica Jawahir and Lon Chubiz for critical comments on the manuscript.

Received March 14, 2019; accepted April 25, 2019; published May 28, 2019.

LITERATURE CITED

Adham AR, Zolman BK, Millius A, Bartel B (2005) Mutations in *Arabidopsis* acyl-CoA oxidase genes reveal distinct and overlapping roles in β-oxidation. Plant J **41:** 859–874

Allenbach L, Poirier Y (2000) Analysis of the alternative pathways for the beta-oxidation of unsaturated fatty acids using transgenic plants synthesizing polyhydroxyalkanoates in peroxisomes. Plant Physiol **124:** 1159–1168

Böttcher C, Pollmann S (2009) Plant oxylipins: Plant responses to 12-oxophytodienoic acid are governed by its specific structural and functional properties. FEBS J **276:** 4693–4704

Clough SJ, Bent AF (1998) Floral dip: A simplified method for Agrobacterium-mediated transformation of *Arabidopsis thaliana*. Plant J **16:** 735–743

De Marcos Lousa C, van Roermund CW, Postis VL, Dietrich D, Kerr ID, Wanders RJ, Baldwin SA, Baker A, Theodoulou FL (2013) Intrinsic acyl-CoA thioesterase activity of a peroxisomal ATP binding cassette transporter is required for transport and metabolism of fatty acids. Proc Natl Acad Sci USA **110:** 1279–1284

Eastmond PJ (2006) *SUGAR-DEPENDENT1* encodes a patatin domain triacylglycerol lipase that initiates storage oil breakdown in germinating *Arabidopsis* seeds. Plant Cell **18:** 665–675

Fan J, Yan C, Xu C (2013) Phospholipid:diacylglycerol acyltransferase-mediated triacylglycerol biosynthesis is crucial for protection against fatty acid-induced cell death in growing tissues of Arabidopsis. Plant J **76:** 930–942

Feiguelman G, Fu Y, Yalovsky S (2018) ROP GTPases structure-function and signaling pathways. Plant Physiol **176:** 57–79

Footitt S, Slocombe SP, Larner V, Kurup S, Wu Y, Larson T, Graham I, Baker A, Holdsworth M (2002) Control of germination and lipid mobilization by COMATOSE, the Arabidopsis homologue of human ALDP. EMBO J **21:** 2912–2922

Fu Y, Gu Y, Zheng Z, Wasteneys G, Yang Z (2005) Arabidopsis interdigitating cell growth requires two antagonistic pathways with opposing action on cell morphogenesis. Cell **120:** 687–700

Fulda M, Schnurr J, Abbadi A, Heinz E, Browse J (2004) Peroxisomal Acyl-CoA synthetase activity is essential for seedling development in *Arabidopsis thaliana*. Plant Cell **16:** 394–405

Ge X, Dietrich C, Matsuno M, Li G, Berg H, Xia Y (2005) An *Arabidopsis* aspartic protease functions as an anti-cell-death component in reproduction and embryogenesis. EMBO Rep **6:** 282–288

Germain V, Rylott EL, Larson TR, Sherson SM, Bechtold N, Carde J-P, Bryce JH, Graham IA, Smith SM (2001) Requirement for 3-ketoacyl-CoA thiolase-2 in peroxisome development, fatty acid β-oxidation and breakdown of triacylglycerol in lipid bodies of Arabidopsis seedlings. Plant J **28:** 1–12

Goepfert S, Hiltunen JK, Poirier Y (2006) Identification and functional characterization of a monofunctional peroxisomal enoyl-CoA hydratase 2 that participates in the degradation of even cis-unsaturated fatty acids in *Arabidopsis thaliana*. J Biol Chem **281:** 35894–35903

Goepfert S, Vidoudez C, Tellgren-Roth C, Delessert S, Hiltunen JK, Poirier Y (2008) Peroxisomal Delta(3),Delta(2)-enoyl CoA isomerases and evolution of cytosolic paralogues in embryophytes. Plant J **56:** 728–742

Graham IA (2008) Seed storage oil mobilization. Annu Rev Plant Biol **59:** 115–142

Haughn GW, Somerville C (1986) Sulfonylurea-resistant mutants of *Arabidopsis thaliana*. Mol Gen Genet **204:** 430–434

Hayashi M, Toriyama K, Kondo M, Nishimura M (1998) 2,4-Dichlorophenoxybutyric acid-resistant mutants of *Arabidopsis* have defects in glyoxysomal fatty acid β-oxidation. Plant Cell **10:** 183–195

Hayashi M, Nito K, Takei-Hoshi R, Yagi M, Kondo M, Suenaga A, Yamaya T, Nishimura M (2002) Ped3p is a peroxisomal ATP-binding cassette transporter that might supply substrates for fatty acid β-oxidation. Plant Cell Physiol **43:** 1–11

Hu J, Baker A, Bartel B, Linka N, Mullen RT, Reumann S, Zolman BK (2012) Plant peroxisomes: Biogenesis and function. Plant Cell **24:** 2279–2303

Kao YT, Gonzalez KL, Bartel B (2018) Peroxisome function, biogenesis, and dynamics in plants. Plant Physiol **176:** 162–177

Kasuya F, Igarashi K, Fukui M (1996) Inhibition of a medium chain acyl-CoA synthetase involved in glycine conjugation by carboxylic acids. Biochem Pharmacol **52:** 1643–1646

Katano M, Takahashi K, Hirano T, Kazama Y, Abe T, Tsukaya H, Ferjani A (2016) Suppressor screen and phenotype analyses revealed an emerging role of the monofunctional peroxisomal enoyl-CoA hydratase 2 in compensated cell enlargement. Front Plant Sci **7:** 132

Khan BR, Adham AR, Zolman BK (2012) Peroxisomal Acyl-CoA oxidase 4 activity differs between *Arabidopsis* accessions. Plant Mol Biol **78:** 45–58

Kim S, Yamaoka Y, Ono H, Kim H, Shim D, Maeshima M, Martinoia E, Cahoon EB, Nishida I, Lee Y (2013) AtABCA9 transporter supplies fatty acids for lipid synthesis to the endoplasmic reticulum. Proc Natl Acad Sci USA **110:** 773–778

Koncz C, Schell J (1986) The promoter of the TL-DNA gene 5 controls the tissue-specific expression of chimaeric genes carried by a novel type of Agrobacterium binary vector. Mol Gen Genet **204:** 383–396

Lee KR, Chen GQ, Kim HU (2015) Current progress towards the metabolic engineering of plant seed oil for hydroxy fatty acids production. Plant Cell Rep **34:** 603–615

Li M, Bahn SC, Guo L, Musgrave W, Berg H, Welti R, Wang X (2011) Patatin-related phospholipase pPLAIIIβ-induced changes in lipid metabolism alter cellulose content and cell elongation in Arabidopsis. Plant Cell **23:** 1107–1123

Li-Beisson Y, Shorrosh B, Beisson F, Andersson MX, Arondel V, Bates PD, Baud S, Bird D, Debono A, Durrett TP, et al (2010) Acyl-lipid metabolism. The Arabidopsis Book **8:** e0133

Lingard MJ, Bartel B (2009) Arabidopsis LON2 is necessary for peroxisomal function and sustained matrix protein import. Plant Physiol **151:** 1354–1365

Liu Y, Wang X (2016) Extraction and profiling of plant polar glycerol lipids. Bio Protoc **6:** e1849

Liu Y, Wang G, Wang X (2015) Role of aminoalcoholphosphotransferases 1 and 2 in phospholipid homeostasis in Arabidopsis. Plant Cell **27:** 1512–1528

Lunn D, Smith GA, Wallis JG, Browse J (2018) Development defects of hydroxy-fatty acid-accumulating seeds are reduced by castor acyltransferases. Plant Physiol **177:** 553–564

Majda M, Robert S (2018) The role of auxin in cell wall expansion. Int J Mol Sci **19:** E951

Möller B, Poeschl Y, Plötner R, Bürstenbinder K (2017) PaCeQuant: A tool for high-throughput quantification of pavement cell shape characteristics. Plant Physiol **175:** 998–1017

Nyathi Y, De Marcos Lousa C, van Roermund CW, Wanders RJA, Johnson B, Baldwin SA, Theodoulou FL, Baker A (2010) The Arabidopsis peroxisomal ABC transporter, comatose, complements the Saccharomyces cerevisiae pxa1 pxa2Delta mutant for metabolism of long-chain fatty acids and exhibits fatty acyl-CoA-stimulated ATPase activity. J Biol Chem **285:** 29892–29902

O'Neill CM, Gill S, Hobbs D, Morgan C, Bancroft I (2003) Natural variation for seed oil composition in *Arabidopsis thaliana*. Phytochemistry **64:** 1077–1090

Pinfield-Wells H, Rylott EL, Gilday AD, Graham S, Job K, Larson TR, Graham IA (2005) Sucrose rescues seedling establishment but not germination of *Arabidopsis* mutants disrupted in peroxisomal fatty acid catabolism. Plant J **43:** 861–872

Preisig-Müller R, Gühnemann-Schäfer K, Kindl H (1994) Domains of the tetrafunctional protein acting in glyoxysomal fatty acid beta-oxidation. Demonstration of epimerase and isomerase activities on a peptide lacking hydratase activity. J Biol Chem **269:** 20475–20481

Reumann S, Babujee L, Ma C, Wienkoop S, Siemsen T, Antonicelli GE, Rasche N, Lüder F, Weckwerth W, Jahn O (2007) Proteome analysis of Arabidopsis leaf peroxisomes reveals novel targeting peptides, metabolic pathways, and defense mechanisms. Plant Cell **19:** 3170–3193

Richmond TA, Bleecker AB (1999) A defect in β-oxidation causes abnormal inflorescence development in *Arabidopsis*. Plant Cell **11:** 1911–1924

Rinaldi MA, Patel AB, Park J, Lee K, Strader LC, Bartel B (2016) The Roles of β-oxidation and cofactor homeostasis in peroxisome distribution and function in *Arabidopsis thaliana*. Genetics **204:** 1089–1115

Rylott EL, Rogers CA, Gilday AD, Edgell T, Larson TR, Graham IA (2003) *Arabidopsis* mutants in short- and medium-chain acyl-CoA oxidase activities accumulate acyl-CoAs and reveal that fatty acid β-oxidation is essential for embryo development. J Biol Chem **278:** 21370–21377

Rylott EL, Eastmond PJ, Gilday AD, Slocombe SP, Larson TR, Baker A, Graham IA (2006) The *Arabidopsis thaliana* multifunctional protein gene (MFP2) of peroxisomal β-oxidation is essential for seedling establishment. Plant J **45:** 930–941

Spiess GM, Hausman A, Yu P, Cohen JD, Rampey RA, Zolman BK (2014) Auxin input pathway disruptions are mitigated by changes in auxin biosynthetic gene expression in Arabidopsis. Plant Physiol **165:** 1092–1104

Stasinopoulos TC, Hangarter RP (1990) Preventing photochemistry in culture media by long-pass light filters alters growth of cultured tissues. Plant Physiol **93:** 1365–1369

Strader LC, Culler AH, Cohen JD, Bartel B (2010) Conversion of endogenous indole-3-butyric acid to indole-3-acetic acid drives cell expansion in *Arabidopsis* seedlings. Plant Physiol **153:** 1577–1586

Strader LC, Wheeler DL, Christensen SE, Berens JC, Cohen JD, Rampey RA, Bartel B (2011) Multiple facets of *Arabidopsis* seedling development require indole-3-butyric acid-derived auxin. Plant Cell **23:** 984–999

Thazar-Poulot N, Miquel M, Fobis-Loisy I, Gaude T (2015) Peroxisome extensions deliver the Arabidopsis SDP1 lipase to oil bodies. Proc Natl Acad Sci USA **112:** 4158–4163

Toshio M, Folke S (1962) A revised medium for rapid growth and bio assays with tobacco tissue cultures. Physiol Plant **15:** 473–497

Velasquez SM, Barbez E, Kleine-Vehn J, Estevez JM (2016) Auxin and cellular elongation. Plant Physiol **170:** 1206–1215

Wiszniewski AA, Zhou W, Smith SM, Bussell JD (2009) Identification of two *Arabidopsis* genes encoding a peroxisomal oxidoreductase-like protein and an acyl-CoA synthetase-like protein that are required for responses to pro-auxins. Plant Mol Biol **69:** 503–515

Woodward AW, Bartel B (2005) The Arabidopsis peroxisomal targeting signal type 2 receptor PEX7 is necessary for peroxisome function and dependent on PEX5. Mol Biol Cell **16:** 573–583

Wu TC, Belteton SA, Pack J, Szymanski DB, Umulis DM (2016) LobeFinder: A convex hull-based method for quantitative boundary analyses of lobed plant cells. Plant Physiol **171:** 2331–2342

Xu T, Wen M, Nagawa S, Fu Y, Chen J-G, Wu M-J, Perrot-Rechenmann C, Friml J, Jones AM, Yang Z (2010) Cell surface- and rho GTPase-based auxin signaling controls cellular interdigitation in Arabidopsis. Cell **143:** 99–110

Zhang C, Halsey LE, Szymanski DB (2011) The development and geometry of shape change in Arabidopsis thaliana cotyledon pavement cells. BMC Plant Biol **11:** 27

Zolman BK, Yoder A, Bartel B (2000) Genetic analysis of indole-3-butyric acid responses in *Arabidopsis thaliana* reveals four mutant classes. Genetics **156:** 1323–1337

Zolman BK, Silva ID, Bartel B (2001) The *Arabidopsis* pxa1 mutant is defective in an ATP-binding cassette transporter-like protein required for peroxisomal fatty acid β-oxidation. Plant Physiol **127:** 1266–1278

Zolman BK, Nyberg M, Bartel B (2007) IBR3, a novel peroxisomal acyl-CoA dehydrogenase-like protein required for indole-3-butyric acid response. Plant Mol Biol **64:** 59–72

Zolman BK, Martinez N, Millius A, Adham AR, Bartel B (2008) Identification and characterization of *Arabidopsis* indole-3-butyric acid response mutants defective in novel peroxisomal enzymes. Genetics **180:** 237–251